ARMY RESEARCH LABORATORY

Morphology Studies of CHDI-Based Urethane Elastomers by Synchrotron X-Ray Diffraction

C. Richard Desper, Catherine A. Byrne, Yingjie Li,
and Benjamin Chu

ARL-TR-683 February 1995

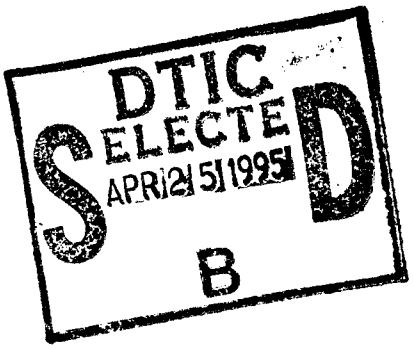

The findings in this report are not to be construed as an official Department of the Army position unless so designated by other authorized documents.

Citation of manufacturer's or trade names does not constitute an official endorsement or approval of the use thereof.

Destroy this report when it is no longer needed. Do not return it to the originator.

REPORT DOCUMENTATION PAGE

Form Approved
OMB No. 0704-0188

1. AGENCY USE ONLY *(Leave blank)*	2. REPORT DATE	3. REPORT TYPE AND DATES COVERED
	February 1995	Final

4. TITLE AND SUBTITLE

Morphology Studies of CHDI-Based Urethane By Synchrotron X-Ray Diffraction

5. FUNDING NUMBERS

6. AUTHOR(S)

C. Richard Desper, Catherine A. Byrne,
*Yingjie Li, and Benjamin Chu

7. PERFORMING ORGANIZATION NAME(S) AND ADDRESS(ES)

Army Research Laboratory
Watertown, MA 02172-0001
ATTN: AMSRL-MA-PB

8. PERFORMING ORGANIZATION REPORT NUMBER

ARL-TR-683

9. SPONSORING/MONITORING AGENCY NAME(S) AND ADDRESS(ES)

10. SPONSORING/MONITORING AGENCY REPORT NUMBER

11. SUPPLEMENTARY NOTES

* Yingjie Li and Benjamin Chu, Department of Chemistry, State University of New York at Stony Brook, Stony Brook, NY 11794-3400

12a. DISTRIBUTION/AVAILABILITY STATEMENT

Approved for public release; distribution unlimited.

12b. DISTRIBUTION CODE

13. ABSTRACT *(Maximum 200 words)*

SEE REVERSE

14. SUBJECT TERMS

Polyurethanes, Multiphase Structure, Annealing Effects, Elastomers, Thermal Analysis

15. NUMBER OF PAGES

53

16. PRICE CODE

17. SECURITY CLASSIFICATION OF REPORT	18. SECURITY CLASSIFICATION OF THIS PAGE	19. SECURITY CLASSIFICATION OF ABSTRACT	20. LIMITATION OF ABSTRACT
Unclassified	Unclassified	Unclassified	UL

NSN 7540-01-280-5500

Standard Form 298 (Rev. 2-89)
Prescribed by ANSI Std. 239-18
298-102

ABSTRACT

Urethane elastomers having hard segments based on CHDI [trans-1,4-diisocyanatocyclohexane] and BD [1,4-butanediol] are notable for their high softening temperatures and low hysteretic heat buildup. Experimental studies as a function of temperature using both wide- and small-angle X-ray diffraction of a series of such elastomers, incorporating PTMO [poly(tetramethylene oxide)] soft segments, reveal the persistence of hard segment microdomains up to 275°C. These hard segment microdomains appear to be paracrystalline at ambient temperature, transforming to a glassy structure above ca. 100°C. That glassy hard segment structure is rigid to at least 275°C, conferring rubbery properties on the material. Electron density variance data obtained by SAXS indicate that there is little hard and soft segment mixing at 30°C for elastomers for which the molar ratio BD/PTMO is less than 2.0, with some segmental mixing indicated for higher BD/PTMO ratios. Changes in the microdomain structure with temperature are, for the most part, reversible for an elastomer with shorter hard segments corresponding to BD/PTMO = 1.5, but show marked irreversibility for one in which BD/PTMO = 3. These results are found to be consistent with models based on model compound data for the hard segment packing.

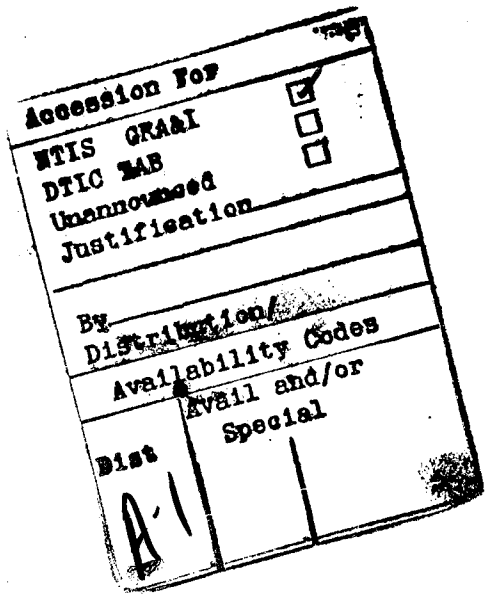

INTRODUCTION

Urethane segmented copolymer elastomers prepared from trans-1,4-diisocyanatocyclohexane (CHDI) and 1,4-butanediol (BD) have been of interest[1] for their high tensile modulus and strength, high tear strength, high softening temperature, and excellent compressive fatigue behavior. In general, urethane elastomers owe their rubbery properties to microphase separation, involving the segretation of hard segments and soft segments into distinct microdomains[2-5] having size parameters in the range of 5 to 20 nm. For elastomers consisting of CHDI/BD hard segments and poly(tetramethylene oxide) (PTMO) soft segments, thermal analysis evidence has indicated the presence of ordered hard segment microdomains, accounting for their superior thermal and mechanical properties.[1] These highly ordered hard segment microdomains result, in turn, from the unusually compact symmetrical structure of the CHDI residue in the hard segment.

The hard segment and the soft segment constituents of the polymer molecule are physically incompatible in their basic thermodynamic parameters, possessing a strong tendency to separate into two phases. However, because the two consituents comprise a block copolymer, with each sequence of a particular constituent being followed by a run of monomers of the other species, the phase separation, if it occurs, must occur at the submicroscopic level. In effect, the domain size of a microphase rich in one or the other molecular

species is limited partially by the dimensions of the individual molecular blocks, confining domains to dimensions in the range of tens to hundreds of Angstroms. The thermal and mechanical properties of such polyurethane elastomers have been studied in terms of this microphase separation model, with the details of the microstructure being elucidated by X-ray diffraction, DSC, and spectroscopic methods. Small-angle X-ray scattering (SAXS) has proven to be particularly useful[2-13] for studying the microphase separation in these materials.

A segmented urethane polymer is elastic for temperatures in which the soft segment microphase is rubbery in character, while the hard segment microphase is glassy or crystalline. Accordingly, such a polymer has as an upper bound of its elastomeric properties the temperature at which the hard segment microphase loses its rigidity. This would be, as the case may be for the particular polymer, either the hard segment glass transition temperature or its crystalline softening temperature. Crystallization, however, is not essential for elastomeric properties, provided that the hard segment glass transition temperature is acceptably high. As an example, in the widely studied class of urethane elastomers whose hard segments are composed of 4,4'-diphenylmethyldiisocyanate (MDI) and 1,4-butanediol (BD), elastomeric properties have been seen in conjunction with crystalline hard segments[13-17]; or in conjunction with glassy, non-crystalline hard segments[2,3,18]. The question of whether a particular urethane in this class, or in any other class, will crystallize, depends upon the details of the hard segment composition and of the thermomechanical history of the polymer. For the MDI / BD class, hydrogen bonding between NH and carbonyl has been demonstrated by Bonart et al[3]. The energetics of this interaction provides an important contribution to the thermodynamic driving force related to the microphase separation process, favoring association of like chemical repeat units rather than mixing of dissimilar chemical repeat units. The structure of the hard segment microphases may, in different instances, be glassy, or show three-dimensional crystallinity or a structure of intermediate two-dimensional order.

The Bonart paracrystalline model[2-3] postulates a defective structure characterized by parallel ordering of hard segment chains in two dimensions.

The improved opportunity for hydrogen bonding interactions, compared to the glassy state, results in improved microphase separation and a higher temperature limit for elasticity. However, hydrogen bonding is not essential for elastomeric behavior in a polyurethane. Certain urethane elastomers containing hard segments composed of piperazine and 1,4-butanediol bischloroformate [Harrell[19]; Allegrezza et al[20]], where the usual NH or OH to carbonyl hydrogen bonding is precluded by the lack of a hydrogen on the piperazine nitrogen, have shown elastomeric properties. Furthermore, recent theoretical molecular simulation work[21] suggests that entropic effects may contribute significantly to the free energy driving the microphase separation process. Thus hydrogen bonding is not, of itself, essential to microphase separation.

The subject of the present work is the class of urethane elastomers in which the hard segment is the reaction product of trans-1,4-diisocyanatocyclohexane (CHDI) and 1,4-butanediol (BD). The thermal and mechanical properties of elastomers of this class have been reported by Siegmann et al[22] and by Byrne et al[23]. The important characteristic of these elastomers, responsible for their continuing interest, is their high temperature mechanical properties. As indicated by both Rheovibron and Thermomechanical Analysis, the elastomeric properties of elastomers in this class persist to temperatures well above those at which more conventional urethane elastomers, such as those of the MDI / BD class, give out. Both the Siegmann and the Byrne papers contain wide angle X-ray diffraction data which show, in some instances, preliminary evidence of hard segment crystallization, consisting of small crystalline peaks superimposed on a strong amorphous halo. One factor leading to difficulties in observing hard segment crystallization in such patterns is the low weight fraction of hard segment, around 20%, in typical elastomers of this class. Thus the hard segment pattern must be observed as a small contribution in the presence of a strong soft segment pattern from the 80% poly(tetramethylene oxide) (PTMO) in the formulations used by Siegmann and by Byrne. The latter is typically amorphous, but can show soft segment crystallinity when PTMO segmental molecular weights approaching 3000 are used.

The hard segment structures of urethanes based on CHDI have also been studied by Jasinski[24] using the model compound approach involving the conden-

sation products of CHDI with a monofunctional alcohol. Such compounds are white crystalline solids of quite high melting points: the dimethoxy compound melted at 270°C, while the di-n-butoxy compound showed evidence of decomposition, but not of melting, in the 230- 277°C range. The computer modeling results of Jasinski,[24] based on single crystal X-ray diffraction studies of such model compounds, show quite strong thermodynamic interactions on a theoretical basis, pointing to highly energetic interactions the analogous hard segment species, which are responsible for the high temperature mechanical properties observed in this class of urethane elastomers.

EXPERIMENTAL CONDITIONS

Urethane Elastomer Samples

Polymerization was accomplished by using a two-step, prepolymer method. The soft segment oligomer, poly(tetramethylene oxide) (PTMO) was degassed by heating at 100°C for one hour with stirring and vacuum, at which point the required amount of melted trans-1,4-diisocyanatocyclohexane (CHDI) was added all at once. This mixture was reacted, with stirring under nitrogen, for 1.5 hours, or until a titration of the isocyanate group indicated its theoretical endpoint value to within 0.3%. Next, The 1,4-butanediol (BD) chain extender, preheated to 100°C, was mixed with the prepolymer rapidly for one minute, at which point the mixture was degassed and poured into a mold with a cavity of dimensions 152.4 x 152.4 x 1.3 mm. The mold was transferred first to a hot press (100°C, 100 psi, 1 hour), then removed from the press for an additional 15 hours of cure in a 100°C oven.

The polymer compositions are shown in Table 1. The polymers consisted of (a) a series having a fixed BD/PTMO ratio of 1.5, an (approximately) fixed PTMO M_n of 2000, while the NCO/OH ratio varies between 0.85 and 1.20 because of variation in the CHDI molar content; and (b) a series having a fixed NCO/OH ratio of 1.00, with varied CHDI/PTMO ratios between 2.0 and 5.0, with PTMO M_n values of ca. 2000 or 2900. It was not possible to hold the PTMO M_n value strictly constant, since occasionally a given lot of PTMO would be exhausted. Although we shall designate a series of polymers as having a certain nominal

PTMO M_n value, e.g. 2000, the correct M_n for a specified polymer is used in calculations.

X-ray Diffraction Apparatus

Experimental X-ray diffraction data were obtained in both the small-angle and wide-angle ranges at the X3A2 beamline of the National Synchrotron Light Source (NSLS), located at the Brookhaven National Laboratory in Upton, New York. The experimental setup comprised (1) a primary beam collimation system[25], (2) a sample heating cell, (3) a vacuum flight path, (4) and a Braun position-sensitive proportional counter interfaced via a Camac multiple channel analyzer (MCA) module to a Microvax II computer. Either wide- or small-angle diffraction patterns could be measured by positioning the detector at different distances from the sample. A heating chamber was used for varying sample temperature, which was held fixed to within 1°C as each pattern was obtained. Between patterns,the temperature could be changed at an average rate of 15°/min. In all cases a wavelength of 0.154 nm (1.54 Å) was used.

The X-ray diffraction apparatus used in the synchrotron experiments included a modified Kratky block collimator in the primary beam collimation system[25] to reduce parasitic scattering. However, the beam length d was kept quite small to effectively eliminate the slit-length smearing effect. Thus the data was equivalent to data from "pinhole" collimation, in the sense that no desmearing correction was needed. For convenience, such data shall be referred to as "pinhole" optics data, even though the beam cross-section was rectangular.

Additional small-angle X-ray scattering patterns were obtained using a Kratky camera fitted with a Technology for Energy Corporation position-sensitive proportional counter with a conventional X-ray generator at the U.S. Army Research Laboratory. This instrument does not provide desmeared data; rather it provides data representative of the infinite-slit-smeared case. The conventional SAXS instrument afforded a much wider angular range, to $q = 3.5\ nm^{-1}$ instead of $1.2\ nm^{-1}$ for the Brookhaven instrument used for the SAXS work. Thus the Kratky camera data extends much further into the Porod tail region and is

more suitable for accurate determination of values of the Porod invariant. The Kratky camera data is used only for determining such derived numerical quantities, where desmearing of the data is not required. No effort was made to desmear the Kratky camera data, since their only use was for calculating the electron density variance, for which an equation involving the infinite-slit-smeared intensity was available (see Bonart and Muller[4]).

THEORETICAL TREATMENT OF SAXS DATA

General Remarks

Treatment of the small-angle X-ray scattering data follows, in general terms, previously established methods[7-11]. However, since previous efforts in this area have been presented in difficult and often unclear terms, it was found useful to deal comprehensively with the equations used, relating the concepts systematically and introducing a new concept, the "reduced intensity". Considerable detail is provided in the following discussion to help clarify the methods used and the concepts involved.

All SAXS patterns are reported with respect to the variable $q \equiv h \equiv (4\pi/\lambda) \sin\theta$, where λ is the wavelength (0.154 nm in this work) and 2θ is the scattering angle.

Electron Density Variance (Porod Invariant)

The determination from SAXS data of the average squared electron density fluctuation, the electron density variance $\langle(\Delta\rho_e)^2\rangle'$, has been described by Kratky[26]. The single apostrophe (') in $\langle(\Delta\rho_e)^2\rangle'$, follows the convention of Bonart and Muller4 and of Koberstein and Stein[27] to indicate that the data have been corrected for background and diffuse scattering, but not for nonzero interface thickness which gives departure from Porod's Law in the tail region. The method may be used with either desmeared or infinite-slit-smeared intensity data, and requires an appropriate integration over such data. In addition, a method for the determination of the power of the SAXS primary beam is required in order to place the data in absolute rather than relative terms. For

infinite-slit-smeared data, e.g. when a Kratky camera is used to collect data, a standard sample of Lupolen polyethylene calibrated in Dr. Kratky's laboratory[28] may be used to determine the power of the beam. Different standard samples may be more appropriate for a "pinhole" optics instrument which yields desmeared data directly, such as those commonly used with synchrotron radiation. Appropriate standard samples in this case have been discussed by Russell[29].

For desmeared data, Kratky[26] determines $\langle(\Delta\rho_e)^2\rangle'$ to be:

$$\langle(\Delta\rho_e)^2\rangle' = (8.34\cdot10^{-3}\cdot D\cdot a\cdot P_s)^{-1} \int_0^{+\infty} m^2\, I_K(m)\, dm\ , \qquad (1)$$

where the definitions of the specimen and instrumental variables is given in Table 2. In the above equation, scattered intensity is expressed in terms of Kratky's variable m, which is a linear (rather than angular) parameter, and is instrument-dependent in significance. Assuming that $\sin\theta \simeq \theta$, valid for small angles, the variable m may be transformed to the more fundamental scattering variable q by:

$$q = (2\pi/\lambda)(m/a)\ . \qquad (2)$$

Using this transformation and substituting C_k for $8.34\cdot10^{-3}$ one obtains:

$$\langle(\Delta\rho_e)^2\rangle' = (C_k\cdot D\cdot a\cdot P_s)^{-1}\ (a\lambda/2\pi)^3 \int_0^{+\infty} q^2\, I(q)\, dq\ . \qquad (3)$$

For infinite-slit-smeared data, Kratky[26] writes:

$$\langle(\Delta\rho_e)^2\rangle' = (2\cdot C_k\cdot D\cdot a\cdot P_s)^{-1} \int_0^{+\infty} m\, \tilde{I}_K(m)\, dm\ , \qquad (4)$$

where $\tilde{I}_K(m)$ is the experimental data, which transforms to:

$$\langle(\Delta\rho_e)^2\rangle' = (2 \cdot C_k \cdot D \cdot a \cdot P_s)^{-1} \; (a\lambda/2\pi)^2 \int_0^{+\infty} q \, \tilde{I}(q) \, dq \; . \qquad (5)$$

Extrapolation to Zero and Infinity for Porod Invariant Determination

Whether the data is desmeared or infinite-slit-smeared, however, the integration required to determine the electron density variance has q limits from zero to infinity. Because of obvious instrumental limitations, the experimental data will not extend to either end point, but will be limited to a range $q_L \leq q \leq q_H$. Thus methods may be needed to extrapolate the intensity curves in the low end range $0 \leq q \leq q_L$ and the high end range $q_H \leq q < \infty$. For the low end a Guinier Law (Gaussian) function is used if needed; i.e. if the intensity is rising as q descends into the extrapolation range. For the high end, either Porod's law:

$$I(q) = K_p \cdot q^{-n} \; , \qquad (6)$$

where K_p is a parameter characteristic of the sample, and n is 4 for desmeared and 3 for infinite slit data, or an empirical equation, where the power n is replaced by an empirically determined floating point number, may be used. Once the curve fit parameters are established at either end, the extrapolation contribution to the required integral may be calculated from an analytical expression. In practice, it is preferable that the extrapolation parts of the integral be small compared to the experimental part of the integral. In the present work, the extrapolation to zero angle was omitted for both infinite slit or "pinhole" collimation data, while the extrapolation to infinite angle was used for the infinite-slit-smeared data only. The electron density variance values from the synchrotron data should be used for comparative purposes only; the results from the infinite slit instrument are more accurate. Because of the very wide range available using the Kratky instrument, the extrapolation to infinite angle could be applied at a larger q value, where it had a smaller influence on the total integration for the Porod invariant.

Definition of Absolute SAXS Scattered Intensity $I_{abs}(q)$

There are two different approaches to defining scattered SAXS intensities in absolute terms, namely that of Kratky[26], where the scattered intensity $I_K(m)$ (or better, $I(q)$) is divided by P_s, as in equations (2-5); and that of Russell et al[29], in which a absolute differential scattering cross section per unit volume $d\sigma(q)/d\Omega$ is used. Since the formalism of the two approaches differs, although each is valid in its own context, it is necessary to select one or the other to continue. The Kratky approach has been selected, largely on the basis that its formalism deals with both desmeared and infinite-slit-smeared data. An absolute scattered intensity function $I_{abs}(q)$ is defined as:

$$I_{abs}(q) \equiv (I(q)\ a^2) \ / \ (P_0\ D\ A_s) \qquad (7)$$

for desmeared data, and as $\tilde{I}_{abs}(q)$, for infinite-slit-smeared data):

$$\tilde{I}_{abs}(q) \equiv (\tilde{I}(q)\ a^1) \ / \ (P_0\ D\ A_s)\ . \qquad (8)$$

These functions compensate for the instrumental parameters P_0 and a^P, and the sample parameters D and A_s, yielding a scattering curve characteristic of the sample morphology in both shape and magnitude. The value of the power of "a" in each case reflects the dimensionality of the experimental setup. The primary beam power P_0 incident on the sample is related to its power P_s as transmitted through the sample by:

$$P_s = P_0\ A_s \qquad (9)$$

Koberstein and Stein[27] have defined a "Rayleigh Ratio" R(h) in analogy with light scattering terminology. Comparing R(h) as defined in their equation (3) with $I_{abs}(q)$ defined in (7), the only difference, noting that h and q are equivalent, is that Koberstein and Stein incorporate the sample absorption A_s into their definition of beam power. In the present work, both desmeared and infinite-slit-smeared data may be dealt with conveniently with a single computer program, provided one accounts properly for the dimensionality

of the experiment, which is 2 for the desmeared (synchrotron) instrument vs. 1 for the infinite-slit-smeared (Kratky) instrument.

Primary Beam Power Calibration

We shall deal with absolute intensities only in the context of the Kratky camera data. In the case of infinite-slit-smeared (Kratky) data, the primary beam power is determined by the method of Kratky[28], using the intensity $\tilde{I}_{c,150}$ from the Lupolen standard measured at an angle corresponding to a Bragg d spacing of 150 Å. The primary beam intensity P_s may be calculated from:

$$P_s = C_{Lupolen} \cdot A_s \cdot a_{Lup} \cdot \tilde{I}_{c,150} \ , \qquad (10)$$

using the value of the constant $C_{Lupolen}$ provided with the calibration sample. In (10), a_{Lup} is the value of the distance a at which the Lupolen calibration is performed. This value is usually unchanged when other data sets are measured, but for generality, we shall distinguish between the two.

Definition of the Reduced Intensity Function

Even if one should lack a means of absolute intensity calibration, a method for rendering the data into a form suitable for making useful comparisons between data sets on a relative basis has been devised and put into effect. For this purpose, let us introduce here a "reduced intensity" $I_{red}(q)$, defined as:

$$I_{red}(q) = I(q) \ [a^2 \ / \ (D \ A_s)] \qquad (11)$$

for desmeared data, and:

$$\tilde{I}_{red}(q) = \tilde{I}(q) \ [a^1 \ / \ (D \ A_s)] \qquad (12)$$

for infinite-slit-smeared data. Comparing with (7) and (8), the reduced intensity function contains compensation for the instrument and specimen parameters a, D, and A_s, lacking only the P_0 divisor when compared with the

absolute intensity function. The reduced intensity may be used in place of the absolute intensity for purposes of comparisons on a given instrument, including Porod invariant comparisons, as long as the results are recognized as relative values within a particular set of data, rather than as absolute values.

Compensation for Beam Power Decay

In experiments using the synchrotron radiation source, the decay of the beam power P_0 was monitored by used of an ionization chamber and the data sets were compensated appropriately.

Diffuse Scattering Correction

In all of the aforementioned treatments of the SAXS data, one must correct for diffuse scattering arising from thermal motions and static disorder of the atoms within microdomains before proceeding further with calculations. The method used to determine the diffuse scattering intensity, proposed by Ruland[30], consists of plotting $q^n \cdot I(q)$ versus q^n, where, as in eq. (6), n assumes a value of 3 for infinite-slit-smeared data, 4 for desmeared data. In the Porod tail region, such a plot should follow a straight line with a negative slope; the absolute value of that slope is the diffuse scattering intensity.

Interface Thickness

Depending upon the nature of the material, the boundaries between microphases may not be sharp, but may be characterized instead by a boundary layer of finite (nonzero) thickness. Such an interface boundary can lead to departure from Porod's Law, equation (6), which would otherwise apply in the tail region for a system having sharp boundaries. The determination of the value of such an interface boundary thickness can be fraught with difficulties in terms of evaluating the proper correction to apply for diffuse scattering intensity. Such determinations have been discussed extensively[30-32] and will not be detailed here. Interface thicknesses were determined in the present

work only for the infinite-slit data, using the method of Koberstein, Morra and Stein[31]. In this method, the quantity ln $(\tilde{I}(q) \cdot q^3)$ is plotted against $q^{1.81}$. At higher angles, this plot should become linear with a negative slope, and the interface thickness is calculated from the magnitude of that slope. Note that a system of sharp interface boundaries will show zero slope, while a positive slope indicates that not all of the diffuse scattering intensity has been subtracted.

Quantitative Interpretation of Electron Density Variance

In the simplest case, in which a material consists of two microphases of electron densities ρ_H and ρ_S, and corresponding volume fractions ϕ_H and ϕ_S, respectively, but NO diffuse boundary layer, the electron density variance $\langle(\Delta\rho_e)^2\rangle'$ may be written as:

$$\langle(\Delta\rho_e)^2\rangle' = \phi_H \phi_S (\rho_H - \rho_S)2 = \phi_H (1 - \phi_H) (\rho_H - \rho_S)2 \qquad (13)$$

where the quantities involved are defined in Table 3. The experimental value for $\langle(\Delta\rho_e)^2\rangle'$ is obtained using eqn. (3) or (5), as applicable, for the short slit length (synchrotron) or the infinite slit length (Kratky camera) instrument.

In the case of diffuse boundaries, two approaches have been used. In the first approach, one may modify the Porod Invariant equation to correct the experimental intensity before the indicated integration is performed. Thus Bonart and Muller[4] offer a modified form of eqn. (3) [his eqn. (21)], dividing by a damping factor function obtained from the tail region fit for the interface thickness determination. The resulting equation yields directly a density variance value $\langle(\Delta\rho_e)^2\rangle''$ for an idealized system in which the boundaries are sharp. Note that a double prime ('') is used, following Bonart and Muller,[4] to indicate that the value has been corrected for both diffuse scattering and diffuse microphase boundaries. For the case of the infinite-slit instrument, Leung and Koberstein[31] offer an analogous equation, their (6), in place of the present eqn. (5), which again yields directly the value of $\langle(\Delta\rho_e)^2\rangle''$.

Alternately, one may integrate first, then correct the experimental $\langle(\Delta\rho_e)^2\rangle'$ value as given from (3) or (5) for the effect of diffuse microphase boundaries to calculate $\langle(\Delta\rho_e)^2\rangle''$. Again, this requires an experimental interface thickness value from the tail region fit. Appropriate equation for the purpose, such as Vonk's[34] eqn. (13) or Desper and Schneider's[11] eqn. (16).

For the present urethane elastomers, the correction for a diffuse boundary was found to be unnecessary, as will be demonstrated. The actual boundary layer thicknesses are sufficiently small that they cannot be distinguished experimentally from zero thickness. Consequently, the data were analyzed by ignoring any effect of diffuse boundary layer, in effect equating $\langle(\Delta\rho_e)^2\rangle'$ with $\langle(\Delta\rho_e)^2\rangle''$.

Inhomogeneity Length (Correlation Distance)

The inhomogeneity length or correlation distance L_c, first defined by Porod[7], is a reciprocally averaged length of vectors which span a section of low-density microphase, followed by a section of high-density microphase. Such a quantity may be determined[7] from the ratio of two integrals over all possible values of q:

$$L_c = \pi \int_0^{+\infty} q\, I(q)\, dq \,/\, \int_0^{+\infty} q^2\, I(q)\, dq \qquad (14)$$

for desmeared ("pinhole" optics) data, and

$$L_c = 2 \int_0^{+\infty} \tilde{I}(q)\, dq \,/\, \int_0^{+\infty} q\, \tilde{I}(q)\, dq \qquad (15)$$

for infinite-slit-smeared data. (Note that the constants 2 and π appearing in (14) and (15) reflect the choice of q as the independent variable). One may define L_H and L_S to be the inhomogeneity lengths in the hard or the soft

segment microphases, respectively. If one has knowledge of ϕ_H and ϕ_S, one may calculate L_H and L_S from:

$$L_H = L_C / (1 - \phi_H) \text{ and } L_S = L_C / (1 - \phi_S) \text{ .} \qquad (16)$$

Since the ratio of two integrals is involved, any calibration constants would cancel out, so the intensities involved in the integrations need not be in absolute terms. As for the electron density variance determination, however, some provision may be required to deal with those intensities which are experimentally inaccessible at the low and high ends of the integrations.

Computer Software

One of the present authors (CRD) has written extensive computer software in the Fortran 77 language which was used in processing the data. This software, named MCAMENU, supports all of the corrections and calculations referred to herein, and is particularly convenient for use in applications such as the present heating experiments, where multiple scans, generating multiple data files, are run for a single specimen. The software is user-friendly, menu-driven, supports graphics, and has built-in safeguards to keep track of which corrections have been applied to a particular data file. MCAMENU will be reported separately.

EXPERIMENTAL RESULTS

Crystallization Behavior as Studied by WAXS

Attempts to develop hard segment crystallinity through severe heat treatments have been reported by Byrne, Mead and Desper[23]. Three polymer compositions were used for this purpose, three with molar ratios CHDI:PTMO:BD of 2.5:1:1.5, 3.5:1:2.5; and 4:1:3 and a soft segment M_n of 2000. All of these patterns showed d spacings of 0.45, 0.43, and 0.40 nm superimposed on a strong soft segment amorphous halo. One pattern, for the third polyurethane whose composition corresponded to a particularly long average hard segment sequences, showed additional peaks at d spacings of 0.37 and 0.29 nm. There is

no way of determining whether the multiple peaks result from a single hard segment microdomain structure, or from multiple microdomain structures resulting from hard segment fractionation. On the whole, hard segment crystallinity does not appear to play a significant role vis-a-vis this class of elastomers.

For CHDI:PTMO:BD polymers subjected to a milder heat treatment, the WAXS pattern, though definitely noncrystalline, was found to be temperature dependent. Three WAXS heating experiments were run using synchrotron radiation at temperatures beginning at ca. 30°C, up to a high value of ca. 210°C, and returning to ca. 30°C, using compositions C, D, and H of Table 1. A set of patterns corresponding to composition D is show in Fig. 1; patterns at the other two compositions were comparable. The temperature range was selected because of an exotherm in the DSC pattern around 185°C, originally attributed to hard segment crystallization. The premise of the heating experiment was to induce crystallization by passing through this transition at a slow rate, then returning to room temperature. However, neither the first and last patterns, measured near room temperature, showed the multiple sharp peaks expected of crystalline material. On the other hand, the single maximum seen in the room temperature patterns near $2\theta = 19.3°$ (corresponding to a d spacing of 0.46 nm) was unusually more pointed in shape when compared with the rounded amorphous halo seen in the same range at elevated temperatures. The latter, exemplified by the pattern at 212°C, is a typical amorphous polymer peak.

In general, the WAXS patterns obtained near room temperature have a sharpness at the top of the peak which, although not as sharp as the usual crystalline peaks, is quite different from the rounded amorphous peak seen at elevated temperatures. The sharpness of the peak observed at lower temperatures is suggested to consist of a small, fairly sharp peak originating from paracrystalline hard segment material, superimposed on a rounded amorphous peak. An examination of the patterns obtained at various temperatures in Fig. 1, as well as others not shown for the sake of brevity, obtained at additional intermediate temperatures, reveals that the sharpness of the peak persists from 30°C up to around 100°C with ascending temperature, then reappears again ca. 100°C as the temperature is lowered. Thus the disappearance of the structure responsible for the sharpened peak is definitely reversible. The tem-

perature of disappearance and reappearance of the sharpened peak is always higher than any possible soft segment transitions, so the peak could be associated with the hard segment microphase. The only other published WAXS data for CHDI/BD hard segment polyurethanes, that of Siegmann et al[22], showed the same sharpened peak seen here in their Fig. 5c. The Siegmann elastomer consisted of CHDI and BD forming the hard segment, with HTPB (hydroxy-terminated polybutadiene) as the soft segment. The fact that the hard segment composition is common to both studies, while the soft segment is not, strengthens the assignment of the sharpened peak to the hard segment microphase.

Interface Thickness Determinations

The results of interface thickness σ determinations by SAXS, from the Kratky camera data at 30°C, are shown in Table 4. Such a Koberstein[31] plot, from whose slope at higher q values the interface thickness values were calculated, is shown in Fig. 2. It is seen that the Koberstein plot of Fig. 2 is quite close to horizontal for a quite long range of q values. This behavior is very typical of these particular polyurethane materials. For the curve fits obtained in the outer range of q values (q = 1.6 to 1.9 nm^{-1}, or $q^{1.81}$ = 2.3 to 3.25 $nm^{-1}.81$), ten of the thirteen polyurethanes showed a slight negative slope, indicative of σ values of zero to 0.15 nm. The remaining three polyurethanes showed a very small positive slope, which yields no valid σ value; however, the magnitude of these positive slopes is not significant in terms of the accuracy of the determination.

In any event, no significance can ever be placed in an interface thickness value which is less than or equal to the value of a typical chemical bond in the material. Thus, considering that a carbon-carbon single bond has a bond length of 0.154 nm, no σ value of 0.154 nm or smaller may be considered significantly different from zero. Essentially, the premise of any interface thickness determination method is that the effect of interface thickness may be separated from any effects of scattering resulting from interferences between individual atoms. When the apparent interface thickness value is of the same scale as that of interatomic interferences, the assumption that

small-angle scattering intensity may be mathematically separated from the diffuse scattering intensity no longer applies.

The assumption that the Kratky instrument is acting as an infinite-slit device was checked by a computer calculation based on Kratky, Porod and Skala,[34] using the values for the camera parameters in effect in these experiments. For the slit-collimated Kratky instrument, there is a limiting q, dependent upon slit optics parameters, above which the infinite-slit assumption does not hold.[35] Also, Ruland[36], along with Koberstein and Stein[27], have noted that data analysis for the purpose of determining the interface thickness should be limited to data at q values above any potential second-order maximum. These rules were both observed in the present determinations.

To verify the interface thickness determination method, three data sets from the Lupolen standard polyethylene sample were also analyzed in this manner. The results, shown graphically in Fig. 3 and numerically in Table 5, show interface thickness (σ) values of approximately 0.6 nm. Note that the slope of the Koberstein plots for the Lupolen sample were measured in a lower q range of q = 0.88 to 1.05 nm^{-1}, or $q^{1.81}$ = 0.88 to 1.09 nm^{-1}. With these results in mind, the Koberstein plots for the polyurethanes were re-evaluated, fitting the curves at this lower q range. For this re-evaluation (results not shown), seven of the thirteen polyurethanes show unrealistic positive slopes. This indicates that for the polyurethane samples the asymptotic tail region for determination of σ occurs at higher q values. This is consistent with the general observation that the SAXS curves for the polyurethanes are strong at higher angles than that of the Lupolen, which peaks below 0.3 nm^{-1}. Consequently the asymptotic tail behavior is observed, for the polyurethanes, at the higher q range than for the Lupolen.

The polyurethane interfaces are deemed to be quite sharp in these samples. This is consistent with the soft segment Tg data previously reported[23] for these elastomers, which are quite close to the Tg of the pure soft segment phase, indicating that segmental mixing is minimal.

Microphase Separation as Studied by SAXS: Effect of Composition at 30°C

Fig. 4 shows the SAXS pattern at 30°C of a series of seven polyurethanes of molar ratio BD/PTMO fixed at 1.5, but with the moles of CHDI varied in order to vary the total NCO/OH ratio from 0.85 to 1.15. The SAXS intensity is quite strong, indicative of a well-developed microphase separation morphology. The maximum in the pattern at $q \equiv (4\pi/\lambda) \sin \theta = 0.35$ nm^{-1}, translates as a repeat period of $d \equiv 2\pi/q = 18.0$ nm. The patterns at this temperature for a series with molar composition CHDI:PTMO:BD = N:1:(N-1), with the PTMO nominal molecular weight at 2000, are shown in Fig. 5. Again, the scattering maximum is at approximately $q = 0.35$ nm^{-1}, corresponding to $d = 18.0$ nm. These data indicate that the repeat period is largely insensistive to the hard segment sequence length or to the NCO/OH ratio, which is understandable in view of the relatively small weight fractions of the hard segment involved, as shown in Table 1. Fig. 6, showing SAXS patterns at this temperature for a series of polymers of molar composition CHDI:PTMO:BD = N:1:(N-1), with the PTMO nominal molecular weight M_n now at 2900, shows a slightly shifted peak position at $q = 0.32$ nm^{-1}, corresponding to $d = 19.6$ nm. Thus a 45% increase in soft segment molecular weight resulted in a 9% increase in the small angle period. Referring to Figs. 4-6, however, it is evident that there is a great deal of variability in the strength of the SAXS peak, which is best studied quantitatively through the electron density variance values, obtained by the Porod invariant method.

The experimental electron density variances for the thirteen elastomers, obtained at 30°C, are shown in the second column of Table 6. These data were first tested against the simplest possible model, that of two microphases, each containing pure hard and soft segment species, and with no diffuse boundary layer. For this case eqn. (13) is modified by replacing the electron densities ρ_H and ρ_S with the pure microphase values ρ_{HP} and ρ_{SP}, and the volume fractions ϕH and ϕS with the pure microphase values ϕ_{HP} and ϕ_{SP}:

$$\langle(\Delta\rho_e)^2\rangle P = \phi_{HP}\ \phi_{SP}\ (\rho_{HP} - \rho_{SP})2 = \phi_{HP}\ (1 - \phi_{HP})\ (\rho_{HP} - \rho_{SP})2\ . \quad (17)$$

The soft segment mass and electron densities μ_{SP} and ρ_{SP} are known[4] from studies of other PTMO-containing polyurethanes, but the hard segment mass and electron densities are not known for the present class. However, for the purpose of testing against this simple model sufficient information is available to calculate from (17), knowing the chemical compositions of the elastomers, the apparent electron density difference $(\rho_{HP} - \rho_{SP})$ assuming $\langle(\Delta\rho_e)^2\rangle_p$ may be identified with the experimental variance value $\langle(\Delta\rho_e)^2\rangle'$. Since ρ_{SP} is known for the PTMO soft segment, one may then obtain the hard segment electron density ρ_{HP}, then the mass density μ_{HP}.

However, there is a minor complication which prevents using a direct solution for ρ_{HP}: the composition data gives us the mass fractions MH and MS, while (13) requires volume fractions. Calculation of the volume fractions requires knowledge of the microphase mass densities μ_{HP} and μ_{SP}, which in turn are proportional to the electron densities ρ_{HP} and ρ_{SP}, whose difference is sought. Thus the solution for $(\rho_{HP} - \rho_{SP})$ is implicit rather than explicit, involving a small number of rather simple equations[7] which need not be repeated here. An iterative solution is readily obtained as outlined previously.[7] A Fortran computer program has been written for this purpose; the results are reported in Table 6 as μ_{HP} and ρ_{HP}, the mass and electron densities calculated for the hard segment microphase. (In every case, the iteration converged to within 0.00001 for ρ_{HP} in less than six iterations).

The computed values of μ_{HP} or ρ_{HP} are remarkably consistent for results of this kind, particularly if one excludes the four samples I, J, L, and M, having the common property that the ratio of moles BD to moles PTMO is 2.0 or greater; i.e. for which the hard segments must include species larger than the simple moiety CHDI-BD-CHDI. With these four samples excluded, the calculated values of μ_{HP} range from 1.352 to 1.363 g/cm^3, while the calculated ρ_{HP} values range from 0.695 to 0.704 moles e$^-$/cm^3. This remarkable consistency very much suggests that the calculated μ_{HP} and ρ_{HP} values represent the mass and electron densities of a pure hard segment phase consisting primarily of -CHDI-BD-CHDI-. (It is recognized that, due to the method of synthesis, there will be a distribution in the molar composition of hard segment species, with the stoichiometry reflecting the average composition of the various hard segment

species.) The four excluded samples exhibit lower hard segment mass and electron densities resulting, presumably, from the fact that their hard segment stoichiometry requires a high fraction of species as large as CHDI-BD-CHDI-BD-CHDI, in addition to the species CHDI-BD-CHDI, in the hard segment microphase. The inclusion of significant amounts of the larger species results in a less efficiently packed hard segment microphase.

To further display these results, a second calculation was performed, obtaining calculated electron density variance values employing eqn. (13) with a value of 1.357 g/cm^3, the average of the nine non-excluded iteration results, for μ_H. In effect, we are now using the pure hard segment density values established above to calculate variance values $\langle(\Delta\rho_e)^2\rangle_p$ for the pure microphase, sharp boundary model for comparison with the experimental variances $\langle(\Delta\rho_e)^2\rangle'$. These calculated variances are shown in column 6 of Table 6, while the ratio of experimental to calculated variance values is shown in column 7. For the nine elastomers having BD/PTMO less than 2.0, this ratio ranges from 0.97 to 1.04, equivalent to 1.00 within experimental error, indicating a near perfect level of microphase separation, assuming a microstructure having μ_{HP} and μ_{SP} values of 1.36 and 0.985 g/cm^3, respectively. For the remaining four elastomers, having BD/PTMO greater than or equal to 2.0, the ratio ranges from 0.76 to 0.89; for such ratios we must conclude that either (a) some segmental mixing has occurred, altering either μ_H, μ_S, or both; or (b) there is NO segmental mixing between the microphases, but the actual μ_H value is less than 1.36 g/cm^3. Note that one cannot assume a priori that μ_H will be independent of hard segment length.

Others have used such a ratio of experimental to ideal variance values as a measure of the degree of overall microphase separation. To place these results in perspective, it is instructive to compare the present results to those in the literature. The corresponding ratios reported by Koberstein and Stein[27], for polyurethanes of MDI/BD[37] or TDI/EG,[37] are in the range 0.31 to 0.41, while the ratios reported by Leung and Koberstein[33] for MDI/BD polyurethanes range from 0.17 to 0.37. Van Bogart, Gibson and Cooper[38] report variance ratios ranging from 0.35 to 0.51 for polyurethanes containing MDI/BD. Viewed with respect to these earlier results, all of the present variance

ratios, ranging from 0.76 to 1.04, are seen as quite high, pointing to the conclusion that the CHDI/BD class of urethane elastomers achieves, in general, much better microphase separation than the MDI/BD or TDI/EG classes previously studied.

Microphase Separation as Studied by SAXS: Effect of Temperature

The changes in microphase separation with temperature, in both heating and cooling, are shown in Figs. 7 and 8 for urethanes of compositions D and L as listed in Table 1. The most remarkable aspect of these SAXS patterns is that, on a qualitative basis, there is relatively little change in the patterns between 30 and 275°C. Compare these patterns, for instance, with the recent data of Chu and co-workers[6,12] where, for urethanes having MDI-BD hard segments, the SAXS pattern essentially disappeared at 220°C, at which temperature the homogeneous melt is stable. The present SAXS data are direct evidence of the persistence of microphase separation in the present CHDI/BD urethanes to quite high temperatures, accounting for the quite high softening temperatures reported by Byrne et al[23] for this class of elastomers.

For a more quantitative look at the temperature effects on the microstructure of the present urethanes, the relative values of the electron density variance have been calculated, using the Porod Invariant method, from the SAXS data of Figs. 7 and 8, and are shown in Figs. 9 and 10. Again, the most remarkable feature is the persistence of strong microphase separation, as evidenced by high electron density variance values, to 275°C. This is in marked contrast to analogous data for MDI/BD polyurethanes[12,39], showing a rapid drop in the variance value with increasing temperature in the range 160-200°C. The persistence in the strength of the variance curve with temperature for the CHDI/BD polyurethanes is in agreement with the excellent high temperature mechanical properties previously reported[23] for CHDI/BD polyurethanes.

Both polymers D and L show some irreversibility in their variance vs. temperature curves (Figs. 9 and 10), but of markedly different nature. Comparing the compositions in Table 1, the two polymers differ mostly in the

lengths of their average hard and soft segments. For polymer D, the average hard segment sequence is 2.5 CHDI and 1.5 BD residues; for polymer L, it is 4.0 CHDI and 3.0 BD residues. Polymer L also has the longer soft segment of the two (M_n = 2862 va. 2033); the two effects compensate so that there is only a comparatively small difference in weight fraction hard segment, 0.239 vs. 0.206.

For polymer D, with the shorter hard and soft segments of the two, the variance behavior is quite reversibile in the range 36-185°C, but becomes pronouncedly irreversible in the 185-275°C range. This irreversibility probably results from a hard segment transition, since the 185°C onset of this hysteresis region coincides with that of a hard segment transition previously reported from DSC experiments.[23] Note, however, that the detailed shape of the SAXS curve at 36°C is changed (see Fig. 7) in the process of the heating experiment, particularly in the range below $q = 0.3\ nm^{-1}$. This indicates that certain details of the microstructure have changed in the heating and cooling process, although the invariant value has not. The changes have affected only the lower q region of the SAXS curve, while the invariant is much more sensitive to the higher q region than the lower q region.

The response of polymer D to the temperature cycle may also be illustrated quantitatively, by reference to the starting and ending values of both the invariant and the inhomogeneity length. At the outset, the invariant value, on a relative basis, is 0.894, while the ending value is 0.888; both measured at 36°C. The difference of less than 1% is insignificant and may be attributed to experimental error. On the other hand, the inhomogeneity length is found to increase by over 7% between start and end. Thus it is seen that the overall change in microstructure involves little change in the electron density variance, coupled with a 7% increase in the microstructure size parameter. It is apparent that the scattering entities have become more extended in size - possibly improving their order by lateral accretion - but have not changed in terms of degree of microphase separation.

The variance behavior (Fig. 10) of polymer L, having the longer hard and soft segments, is quite different. In this case, the variance falls off con-

tinuously in the 195-275°C range with rising temperature, but not precipitously: microphase separation is still present at 275°C. As the temperature is lowered, however, the variance does not follow the ascending temperature curve at all, staying well below that curve throughout the cooling cycle to 36°C. The irreversibility in the polymer L case is attributed to nonequilibrium behavior, possibly associated with kinetic effects. Presumably some segmental mixing is occurring with rising temperature above 195°C, but is not recovered in the decreasing temperature curve. Either the original microstructure was not in the equilibrium state, or slow kinetics for the process of reforming the microstructure cause the irreversibility. In terms of numerical parameters, polymer L showed an 11% decrease in the electron density variance, while the inhomogeneity length increased 6% in the heating cycle.

DISCUSSION

The wide angle X-ray diffraction data indicate that a paracrystalline hard segment phase is formed at the 100°C synthesis temperature in these elastomers. When the cured elastomers are heated above the synthesis temperature, some hard segment reorganization takes place as indicated by the DSC thermal transition at 185°C. Hard segment crystallization is difficult; only under such severe conditions as heating for 16 hours at 150-160°C are crystallites showing multiple sharp crystalline peaks observed. The above observations indicate that although the neighboring CHDI / BD residues in the hard segment microphase have quite strong attractions for each other, as suggested by the model compound studies of Jasinski[24], these attractions can be achieved to a great extent by a structure lacking long range crystalline order. Thus the repeating units can pack with sufficient proximity to drop into energy wells, resulting in a paracrystalline structure characterized by a single sharpened diffraction peak at 0.43-0.44 nm. The strength of these local interactions of like hard segment residues is also indicated by the fact that (unlike most other segmented urethanes) the CHDI/BD segmented urethanes do not readily dissolve in solvents. The energy benefit of having like hard-segment neighbors outweighs the entropy benefit of mixing with either soft segment species or with solvent.

The microstructure, as revealed by SAXS, is characterized by sharp interfacial boundaries and high degrees of segmental segregation, considerably higher than that previously observed for other classes of polyurethanes. The polymer separates into effectively pure microphases for the lower molar content of hard segment, while higher hard segment content (BD/PTMO ratio 2.0 and above) results in some segmental mixing, but less than for other classes of polyurethanes. In this discussion it is recognized that there will be a distribution in the length of hard segment species. Stoichiometry will determine the average length of a hard segment sequence, but there will be appreciable content of hard segments with lengths somewhat above and below that average value.[40] Thus a polymer such as K in Table 1, whose hard segment stoichiometry corresponds to the hard segment dimer -CHDI-BD-CHDI-, will nonetheless contain appreciable amounts of both the monomeric hard segment -CHDI- and the trimeric hard segment -CHDI-BD-CHDI-BD-CHDI-, each terminated at both ends by the start of a soft segment. Information as to the actual hard segment length distribution for these polymers is not, however, readily available.

Koberstein and co-authors[27,39] have discussed the morphology of hard segment microphases in terms of the distribution of lengths of hard segment species in the hard segment microdomain. For the classes of hard segments they studied (abbreviated MDI/BD and of TDI/EG) they found it necessary to modify the earlier model of Bonart[3], depicting parallel packing of the hard segment species, by proposing the folding or coiling of hard segments within the hard segment microdomains. This allows the longer hard segment sequences to coexist with shorter sequences in a hard segment microdomain by folding itself back into the microdomain rather than dangling into the soft segment microdomain. Koberstein and Stein[27] find support for this proposal in terms of the values of microdomain thickness and boundary layer thickness derived from SAXS data, and in terms of the melting points of hard segment model compounds.

However, for the present CHDI/BD hard segment polyurethanes, the above considerations of Koberstein may not apply, because of fundamental differences in the nature of the hard segment microdomains. Koberstein bases his discussion on a lamellar microstructure, which may or may not be present in the

CHDI/BD polyurethanes. For instance, in model compound studies[24] for these hard segments, a structure of space group P21/c occurs, in which the chains do not pack in the usual parallel fashion common to polymeric crystals. Instead, the chains pack in a "herringbone" fashion, as shown in Fig. 11, with all of the chains in the a-b plane, but with half of them at an angle of (roughly) 45° with the b axis while the other half make an angle of (roughly) -45°. Thus the two sets of chains cross each other at (approximately) a 90° angle rather than in the parallel fashion that Koberstein assumes for lamellar microstructures.

In Fig. 12, a possible structure for a CHDI/BD hard segment microdomain analogous to that of the P21/c model compound structure is shown schematically, with the species -CHDI-BD-CHDI- represented as a dumbbell. In each dumbbell the cyclohexyl moieties are represented as spheres, and the urethane / aliphatic residue form the connecting bar between the spheres. Successive dumbbells add to the stack offset alternately to the left and the right of a crystal axis, resulting in a columnar morphology, rather than the usual lamellar structure. Thus the soft segments, shown as solid lines in Fig. 12, would splay out in all directions from the central column of the hard segment microphase, connecting with adjacent columnar structures to form an elastomeric network.

The data presently available is not sufficient to verify or contradict the Fig. 12 structure for the hard segment microphases in the elastomers studied. However, it is important to note that the possibility of such strucures implies that one may not need to presume a lamellar microstructure. Furthermore, the basic difference between lamellar structures and columnar structures means that the arguments of Koberstein et al[27,39] regarding folding ot longer hard segments may not apply to urethane elastomers of the CHDI class.

The Fig. 12 structure has only one dimensional order, repeating in the c direction, the direction of stacking of successive layers; the structure does not repeat in within the plane of the layers. Thus the only diffraction spacings one would expect to observe would be the repeat distance between

successive stacks of chains, analogous to the (002) distance of the model compound, and its orders (if any). This predicted repeat value is $d_{002} = c/2 = 0.4288$ nm, in reasonably good agreement with the paracrystalline spacing of 0.46 nm.

It is recognized that an actual polymer will contain a distribution of hard segment lengths. Thus one must consider structures of mixed hard segment lengths as well as structures comprising hard segments all of the same length. Fractionation of hard segments into microdomains each of a single hard segment length could well prove to be a very slow process; thus structures of mixed hard segment lengths could be favored kinetically but disfavored thermodynamically, providing an impetus for reorganization of the microstructure during annealing at elevated temperatures. Further studies of a variety of model compounds would be required to elucidate such effects.

ACKNOWLEDGMENT

This research was sponsored by the U.S. Army Research Laboratory, the U.S. Army Research Office (DAAH0494G0053), and the Department of Energy, #DEFG086ER45237A010. The authors wish to thank the SUNY beamline at the National Synchrotron Light Source, Brookhaven National Laboratory, and Mr. Alex Chin and Dr. Janice Dieter, formerly of the Army Research Laboratory, for their invaluable assistance.

REFERENCES

1. J. W. Deiter and C. A. Byrne, "Aliphatic Polyurethane Elastomers With High Performance Properties", Polym. Eng & Sci., 27, 673 (1987).

2. R. Bonart, "X-Ray Investigations Concerning the Physical Structure of Cross-Linking in Segmented Urethane Elastomers", J. Macromol. Sci.-Phys., B2, 115 (1968).

3. R. Bonart, L. Morbitzer, and G. Hentze, "X-Ray Investigations Concerning the Physical Structure of Cross-Linking in Urethane Elastomers", J. Macromol. Sci.-Phys., B3, 337 (1969).

4. R. Bonart and E. H. Muller, "Phase Separation in Urethane Elastomers as Judged by Low-Angle X-Ray Scattering. I. Fundamentals", J. Macromol. Sci.-Phys., B10, 177 (1974); "Phase Separation in Urethane Elastomers as Judged by Low-Angle X-Ray Scattering. II. Experimental Results", B10, 345 (1974).

5. R. Bonart, L. Morbitzer, and E. H. Muller, "X-Ray Investigations Concerning the Physical Structure of Cross-Linking in Segmented Urethane Elastomers: III. Common structure Principles for Extensions with Aliphatic Diamines and Diols", J. Macromol. Sci.-Phys., B9, 447 (1974).

6. B. Chu, T. Gao, Y. Li, J. Wang, C. R. Desper, and C. A. Byrne, "Microphase Separation Kinetics in Segmented Polyurethanes: Effects of Soft Segment Length and Structure", Macromolecules, 25, 5724 (1992).

7. G. Porod, "Die Rontgenkleinwinkelstreuung von dichtgepackten kolloiden Systemen: I. Teil", Kolloid-Z., 124, 83 (1951); "Die Rontgenkleinwinkelstreuung von dichtgepackten kolloiden Systemen"; Kolloid-Z., 125, 51, (1952); "Die Rontgenkleinwinkelstreuung von dichtgepackten kolloiden Systemen. II. Teil", Kolloid-Z., 125, 108 (1952); "Berichtigung", 133, 51 (1953).

8. A. Guinier and G. Fournet, Small Angle Scattering of X-rays, Wiley, New York, 1955, 157-160.

9. J. W. C. Van Bogart, A. Lilaonitkul, and S. L. Cooper, "Morphology and Properties of Segmented Copolymers", Adv. in Chem., 176, 3 (1979).

10. C. G. Vonk, "Synthetic Polymers in the Solid State", in Small Angle X-ray Scattering, (O. Glatter and O. Kratky, eds.), Academic Press, New York, 1982, 433-466.

11. C. R. Desper and N. S. Schneider, "Microphase Segregation in Segmented Amine-Cured Polyurethanes", in Polymer Alloys III (D. Klempner and K. C. Frisch, eds.), Plenum Publications, New York, 233 (1983).

12. Y. Li, T. Gao, J. Liu, K. Linliu, C. R. Desper, and B. Chu, "Multiphase Structure of a Segmented Polyurethane: Effects of Temperature and Annealing", Macromolecules, 25, 7365 (1992).

13. N. S. Schneider, C. R. Desper, J. L. Illinger, A. O. King, and D. Barr, "Structural Studies of Crystalline MDI-Based Polyurethanes", J. Macromol. Sci.-Phys., B11, 527 (1975).

14. C. E. Wilkes and C. S. Yusek, "Investigation of Domain Structure in Urethane Elastomers by X-Ray and Thermal Methods", J. Macromol. Sci.-Phys., B7, 157 (1973).

15. J. Blackwell and C. D. Lee, "Hard Segment Polymorphism in MDI/Diol Based Polyurethane Elastomers", J. Polym. Sci., Polym. Phys. Edn., 22, 759 (1984).

16. L. Born, J. Crone, H. Hespe, E. H. Muller, and K. H. Wolf, "On the Structure of Polyurethane Hard Segments Based on MDI and 1,4-BD. X-Ray Diffraction Analysis of Oriented Elastomers and of Single Crystals of a Model Compound", J. Polym. Sci, Polym. Phys. Edn., 22, 163 (1984).

17. C. P. Christenson, M. A. Harthcock, M. D. Meadows, H. L. Spell, W. L. Howard, M. W. Creswick, R. E. Guerra, and R. B. Turner, "Model MDI/BD Polyurethanes: Molecular Structure, Morphology, Physical and Mechanical Properties", J. Polym. Sci., Polym. Phys. Edn., 24, 1401 (1986).

18. S. B. Clough and N. S. Schneider, "Structural Studies of Urethane Elastomers", J. Macromol. Sci.-Phys., B2, 553 (1968).

19. L. L. Harrell, Jr., "Segmented Polyurethanes: Properties as a Function of Segment Size and Distribution", Macromolecules, 2, 607 (1969).

20. A. E. Allegrezza Jr., R. W. Seymour, H. N. Ng, and S. L. Cooper, "Segmental Orientation Studies Block Copolymers: 2. Non-Hydrogen Bonded Polyurethanes", Polymer, 15, 433 (1974).

21. H.-J. Tao, C. F. Fan, W. J. MacKnight, and S. L. Hsu, "Application of a Molecular Simulation Technique for Prediction of Phase-Separated Structures of Semirigid Model Polyurethanes", Macromolecules, 27, 1720 (1994).

22. A. Siegmann, D. Cohen, and M. Narkis, "Polyurethane Elastomers Containing Polybutadiene and Aliphatic Diols: Structure-Property Relationships", Polym. Eng. & Sci., 27, 1187 (1987).

23. C. A. Byrne, J. Mead, and C. R. Desper, "Structure Property Relationship of Aliphatic Polyurethane Elastomers Prepared from CHDI", Adv. Urethane Sci. & Tech., 11, 68 (1992).

24. J. P. Jasinski, C. R. Desper, B. A. Zentner, C. A. Byrne, and R. J. Butcher, "The Structures of Dimethyl N,N'-trans-1,4-cyclohexanedicarbamate (I) and Diethyl N,N'-trans-1,4-cyclohexanedicarbamate (II)", Acta Cryst., C44, 1137 (1988).

25. B. Chu, D. Wu, and C. Wu, "Kratky Block-Collimation Small-Angle X-Ray Diffractometer for Synchrotron Radiation", Rev. Sci. Instrum., 58, 1158 (1987).

26. O. Kratky, "Die Messung der Absolutintensitat der diffusen Rontgenkleinwinkelstreuung -- ein Verfahren zur 'Wagung' in makromolekularen Systemen", Z. analyt. Chem., 201, 161 (1964).

27. J. T. Koberstein and R. S. Stein, "Small-Angle X-Ray Scattering Studies of Microdomain Strucute in Segmented Polyurethane Elastomers", J. Polym. Sci., Polym. Phys. Edn., 21, 1439 (1983).

28. O. Kratky, I. Pilz, and P. J. Schmitz, "Absolute Intensity Measurement of Small Angle X-Ray Scattering by Means of a Standard Sample", J. Coll. Interf. Sci., 21, 24 (1966).

29. T. P. Russell, J. S. Lin, S. Spooner, and G. D. Wignall, "Intercalibration of Small-Angle X-Ray and Neutron Scattering Data", J. Appl. Cryst., 21, 629 (1988).

30. W. Ruland, "Small-Angle Scattering of Two-Phase Systems: Determination and Significance of Systematic Deviations from Porod's Law", J. Appl. Cryst., 4, 70 (1971).

31. J. T. Koberstein, B. Morra, and R. S. Stein, "The Determination of Diffuse-Boundary Thickness of Polymers by Small-Angle X-Ray Scattering", J. Appl. Cryst., 13, 34 (1980).

32. R.-J. Roe, "Examination of Errors in the Determination of Phase Boundary Thickness by Small-Angle X-Ray Scattering", J. Appl. Cryst., 15, 182 (1982).

33. L. M. Leung and J. T. Koberstein, "Small-Angle Scattering Analysis of Hard-Microdomain Structure and Microphase Mixing in Polyurethane Elastomers", J. Polym. Sci.: Polym. Phys. Edn., 23, 1883 (1985).

34. O. Kratky, G. Porod, and Z. Skala, "Verschmierung und Entschmierung bei Rontgenkleinwinkeldiagrammen", Acta Physica Austriaca, 13, 76 (1960).

35. L. B. Shaffer and R. W. Hendricks, "Calibration of Polyethylene (Lupolen) as a Wavelength-Independent Absolute Intensity Standard", J. Appl. Cryst., 7, 159 (1974); L. B. Shaffer and R. W. Hendricks, ORNL-TM-4278, Oak Ridge National Laboratory, 1973.

36. W. Ruland, "The Evaluation of the Small-Angle Scattering of Lamellar Two-Phase Systems by Means of Interface Distribution Functions", Colloid Polym. Sci., 255, 417 (1977).

37. Nomenclature: MDI is 4,4'-diphenylmethane diisocyanate; TDI is (in this instance) an 80/20 mixture of 2,4- and 2,6-toluene diisocyanate; BD is 1,4-butanediol; and EG is ethylene glycol.

38. J. W. C. Van Bogart, P. E. Gibson, and S. L. Cooper, "Structure-Property Relationships in Polycaprolactone-Polyurethanes", J. Polym. Sci., Polym. Phys. Edn., 21, 65 (1983).

39. J. T. Koberstein and T. P. Russell, "Simultaneous SAXS-DSC Study of Multiple Endothermic Behavior in Polyether-Based Block Copolymers", Macromolecules, 19, 714 (1986).

40. L. H. Peebles, "Hard Block Length Distribution in Segmented Block Copolymers", Macromolecules, 9, 58 (1976).

APPENDIX

Figure 1. WAXS heating experiment of polyurethane D from Table 1. Temperatures are indicated along the right vertical axis. Scans at intermediate temperatures are omitted, and successive plots are offset by an upwards baseline shift.

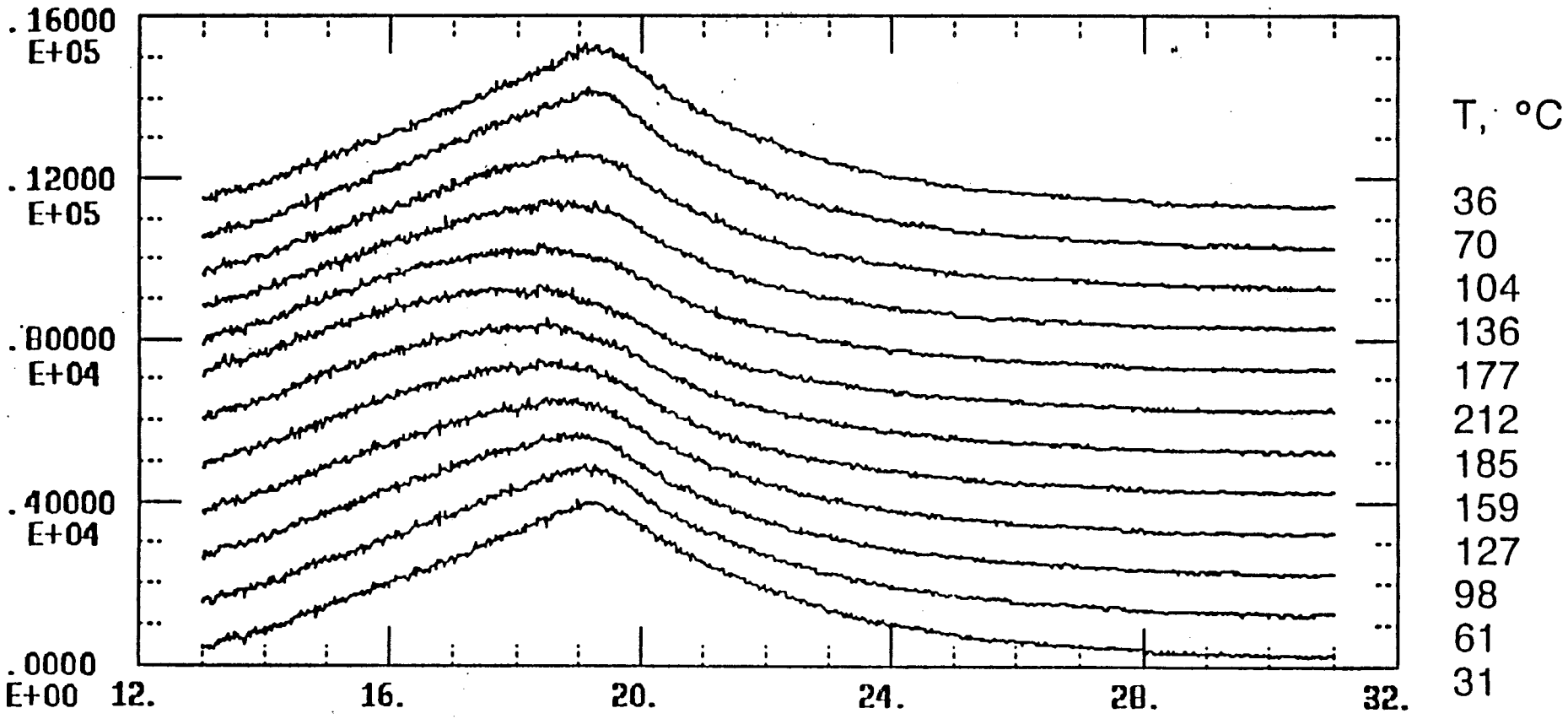

Figure 2. Koberstein[31] plot of SAXS data, obtained using an infinite slit (Kratky) instrument, for polyurethane I.

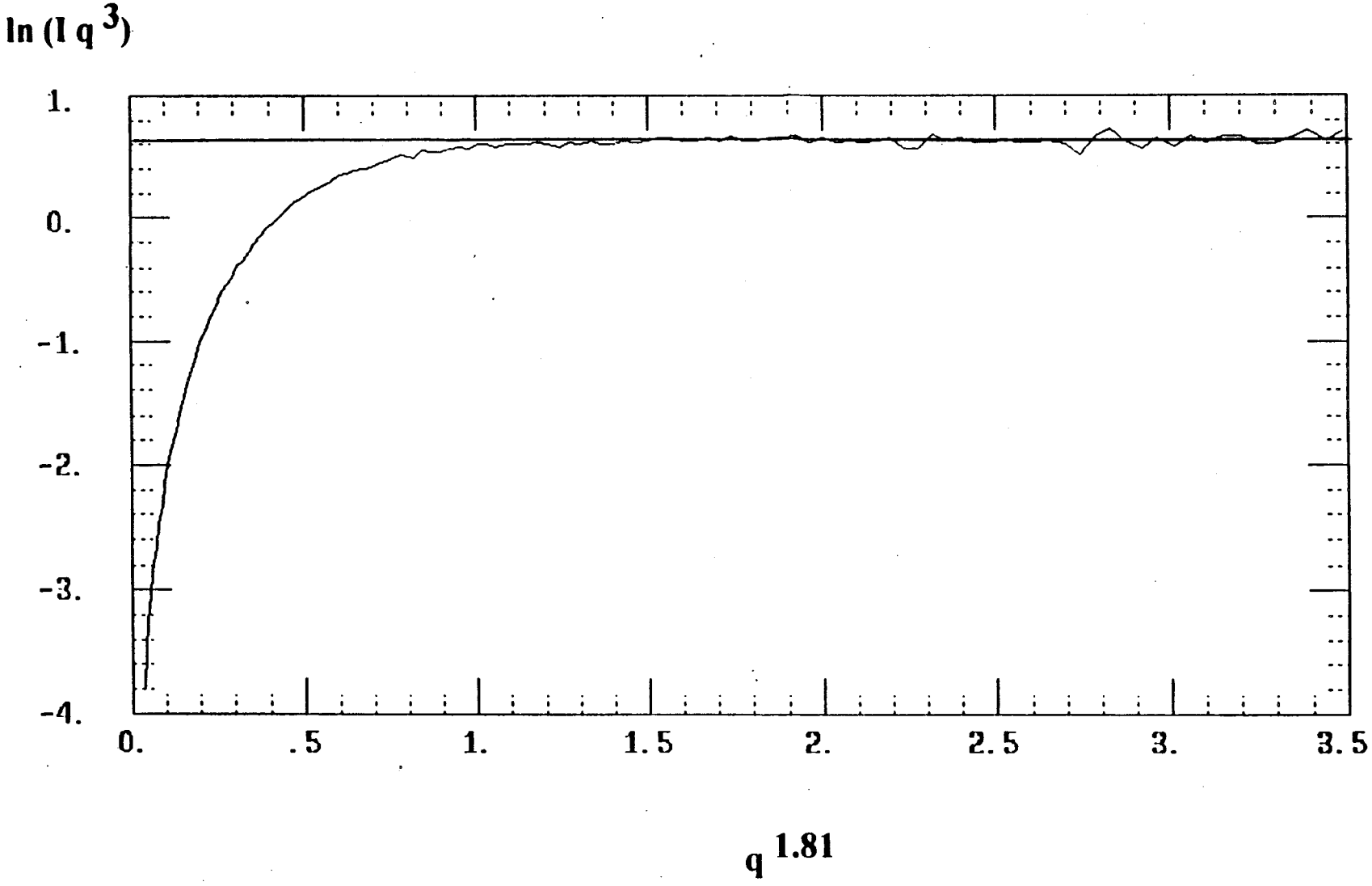

Figure 3. Koberstein[31] plot of SAXS data, obtained using an infinite slit (Kratky) instrument, for a Lupolen polyethylene standard sample.

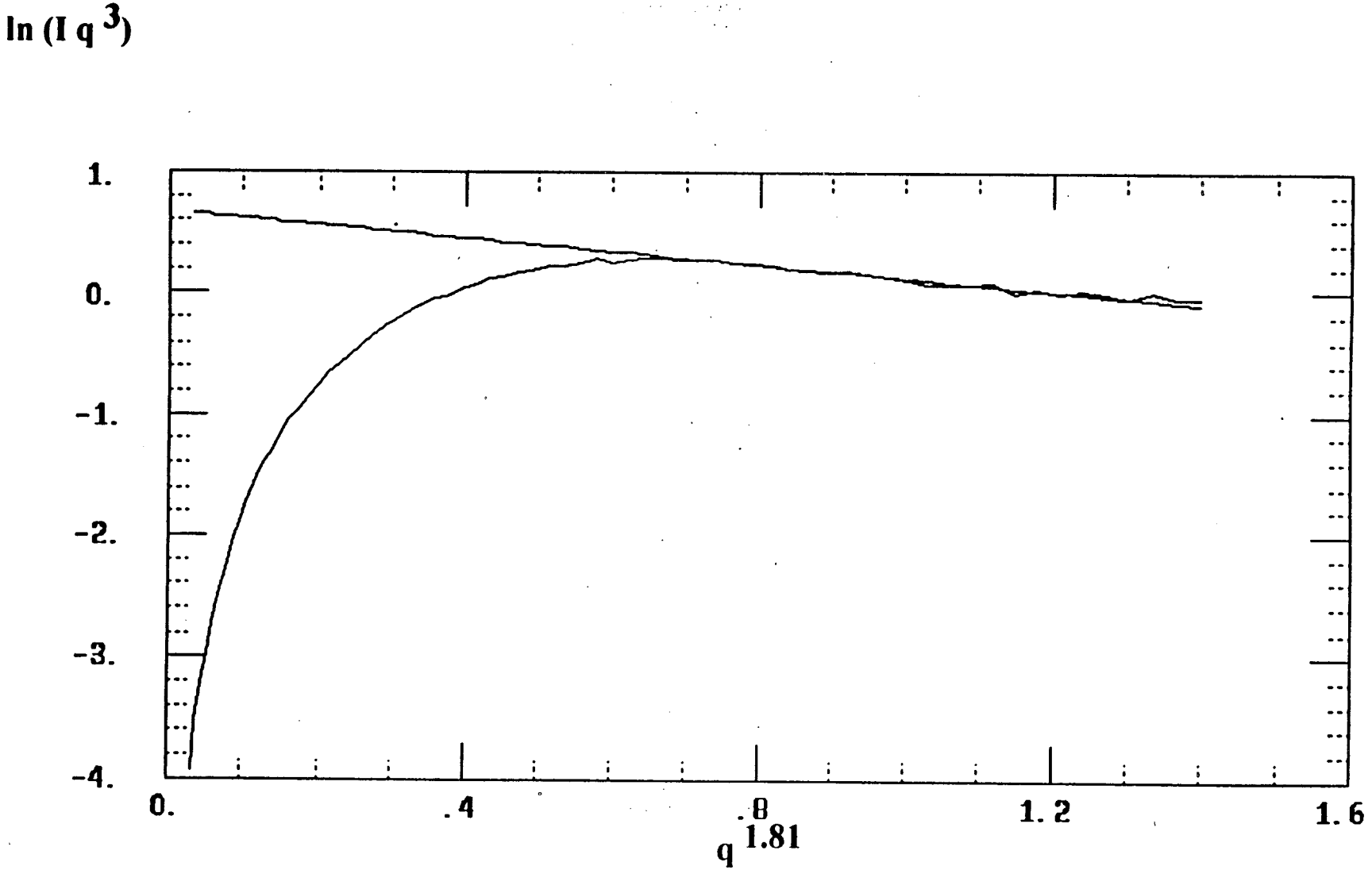

Figure 4. SAXS patterns of polyurethanes A through G (reading from the bottom curve upwards) of Table 1, having NCO/OH ratios from 0.85 to 1.15. The PTMO has a nominal M_n of 2000. Successive plots are offset by an upwards baseline shift.

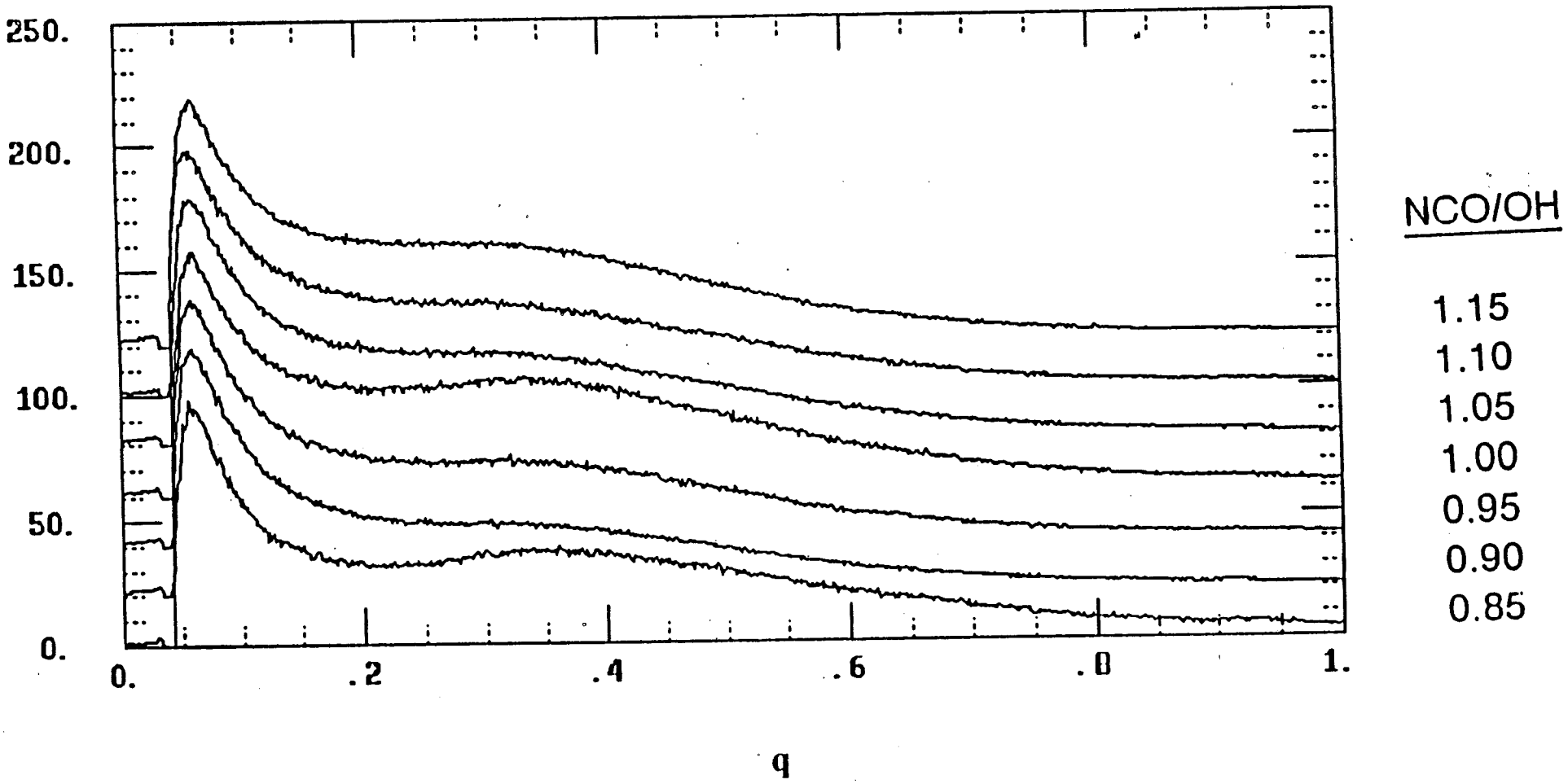

Figure 5. SAXS patterns of polyurethanes D, I, and J (reading from the bottom curve upwards) of Table 1, of composition CHDI:PTMO:BD = N:1:(N–1); the PTMO has a nominal M_n of 2000. The N value is indicated to the right of each plot.

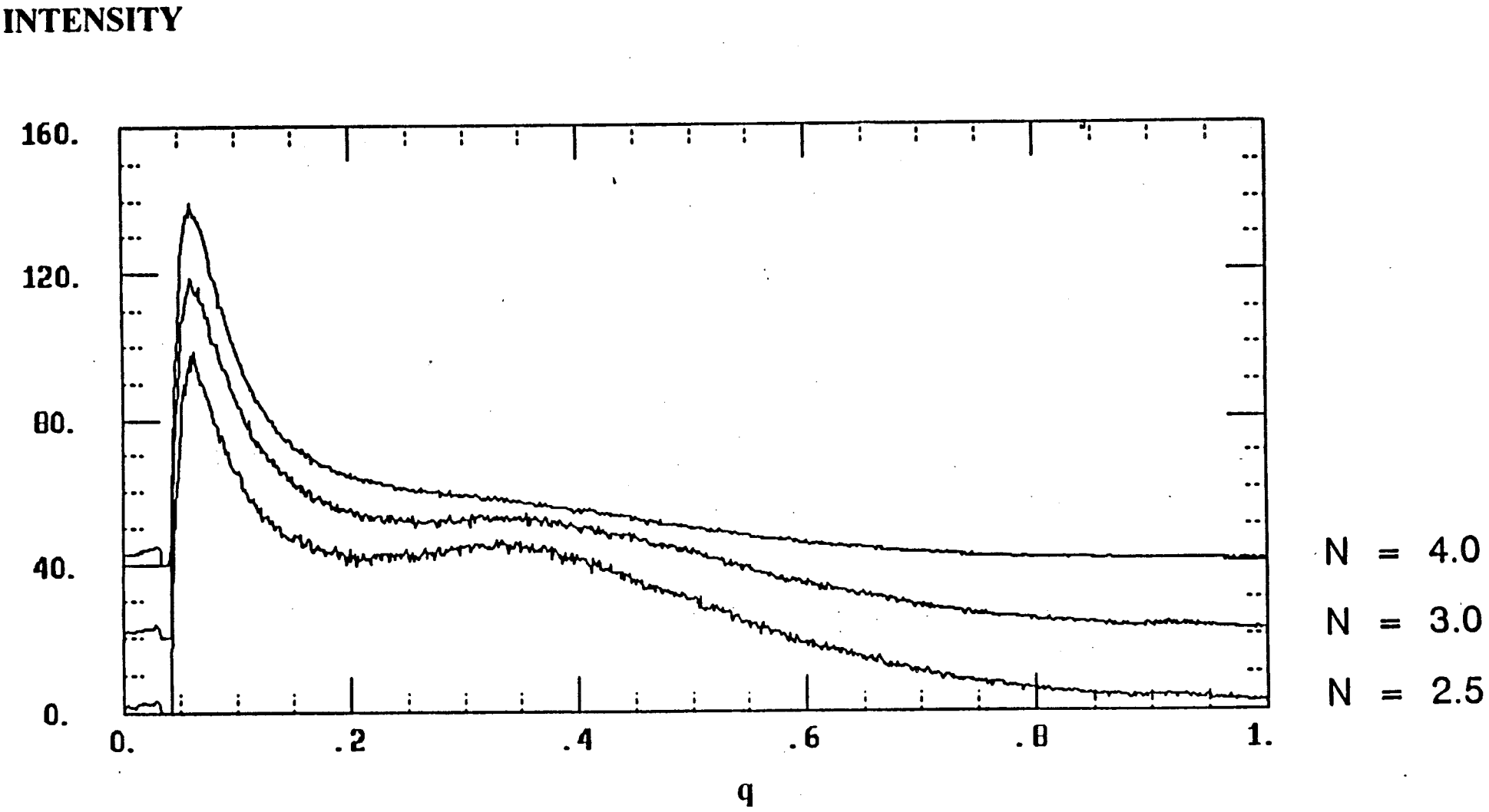

Figure 6. SAXS patterns of polyurethanes K, L, and M (reading from the bottom curve upwards) of Table 1, of composition CHDI:PTMO:BD = N:1:(N-1); the PTMO has a nominal M_n of 2900. The N value is indicated to the right of each plot.

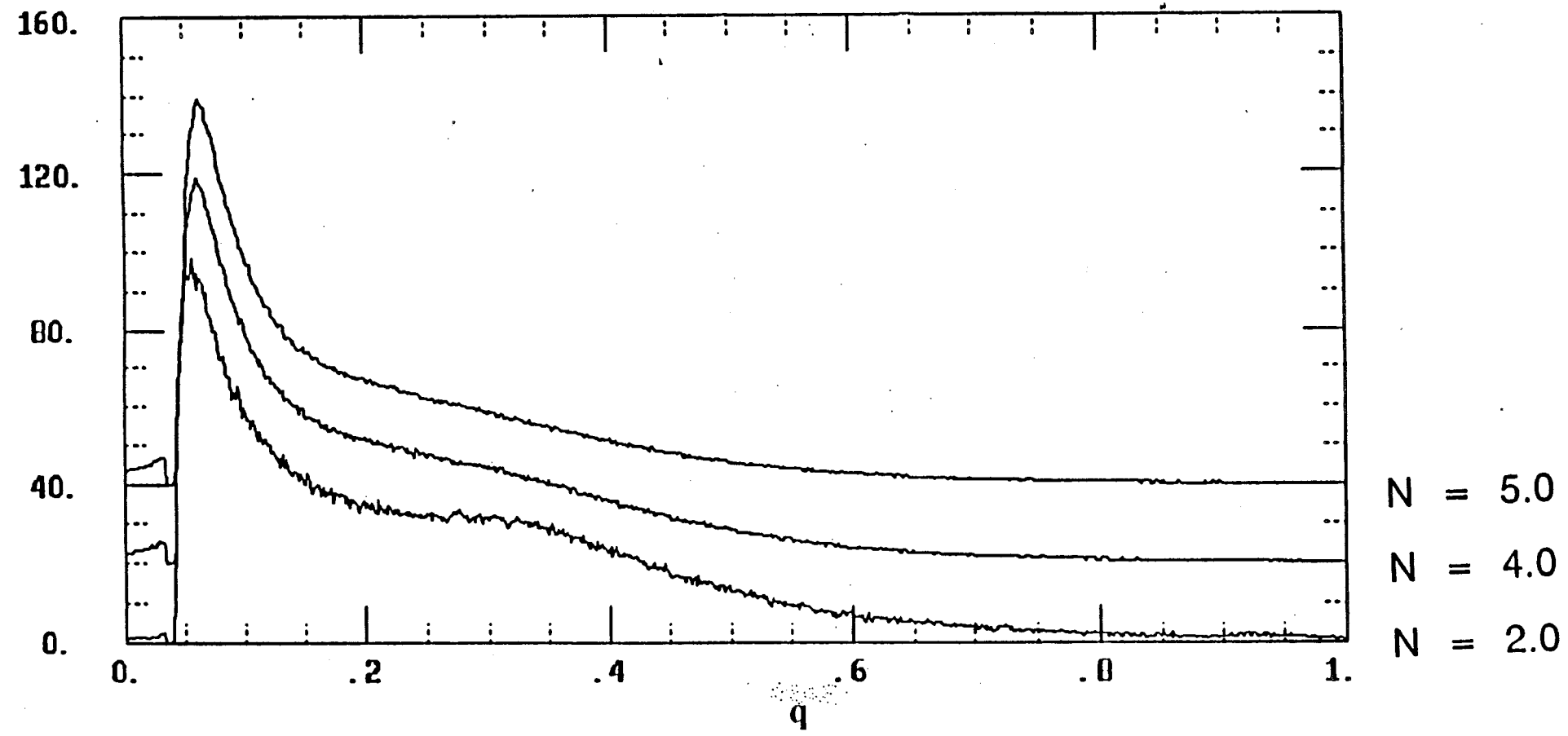

Figure 7. SAXS heating experiment of polyurethane D from Table 1. Temperatures are indicated along the right vertical axis. Scans at intermediate temperatures are omitted, and successive plots are offset by an upwards baseline shift.

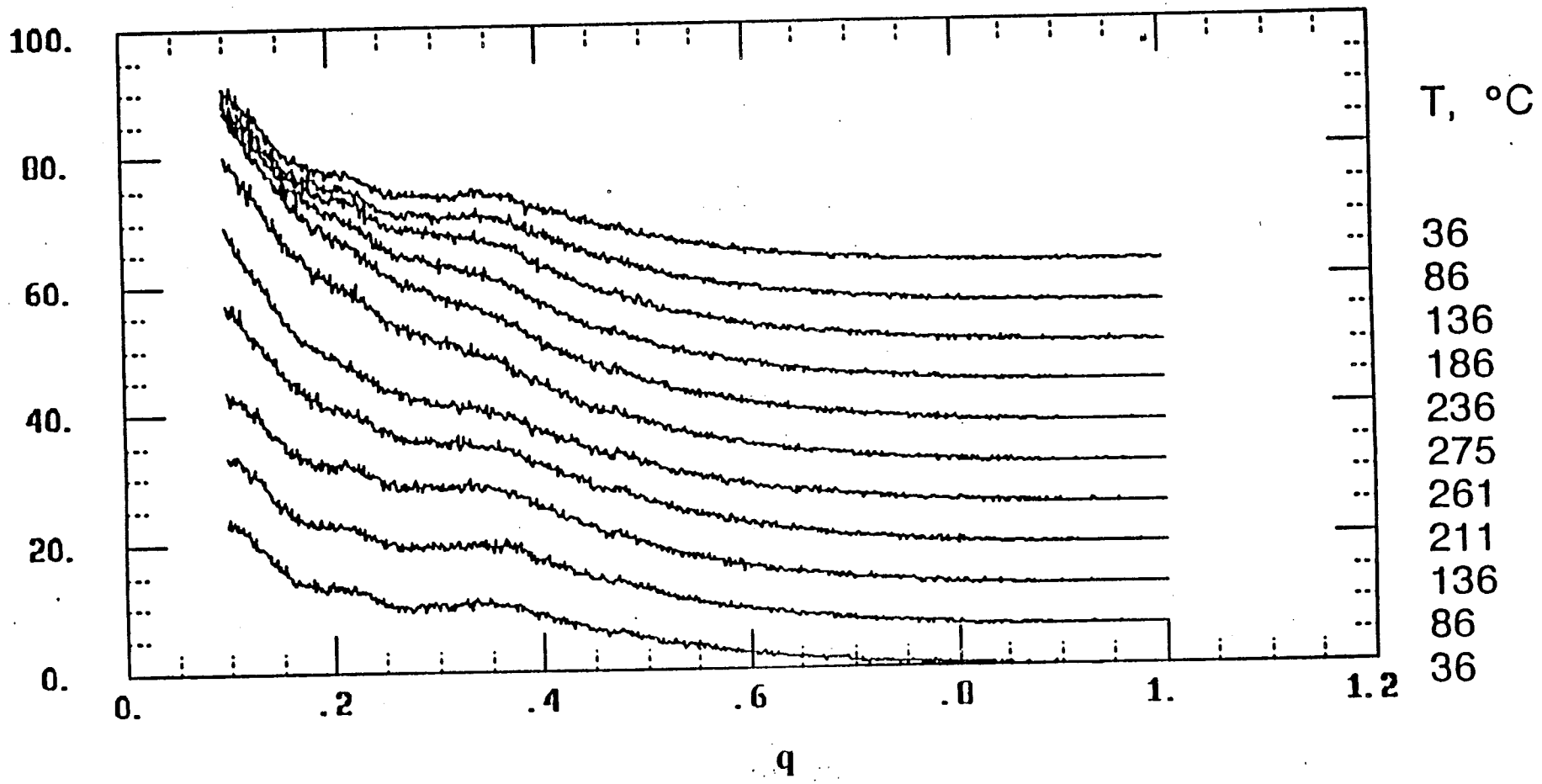

Figure 8. SAXS heating experiment of polyurethane L from Table 1. Scans at intermediate temperatures are omitted, and successive plots are offset by an upwards baseline shift.

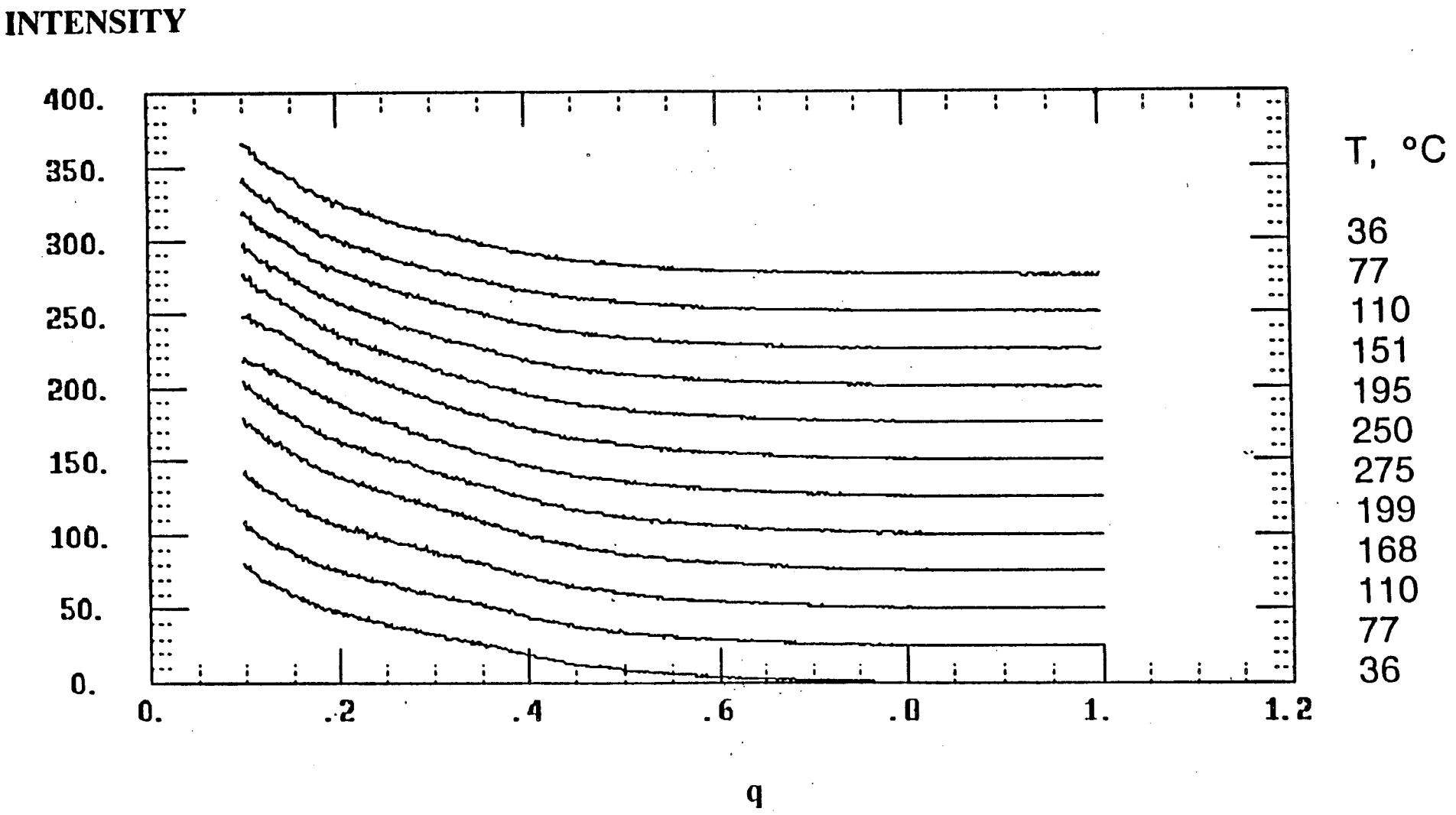

Figure 9. Relative values of Electron Density Variance for the SAXS heating experiment of Figure 5, polyurethane D. Solid line (+): ascending tempera-

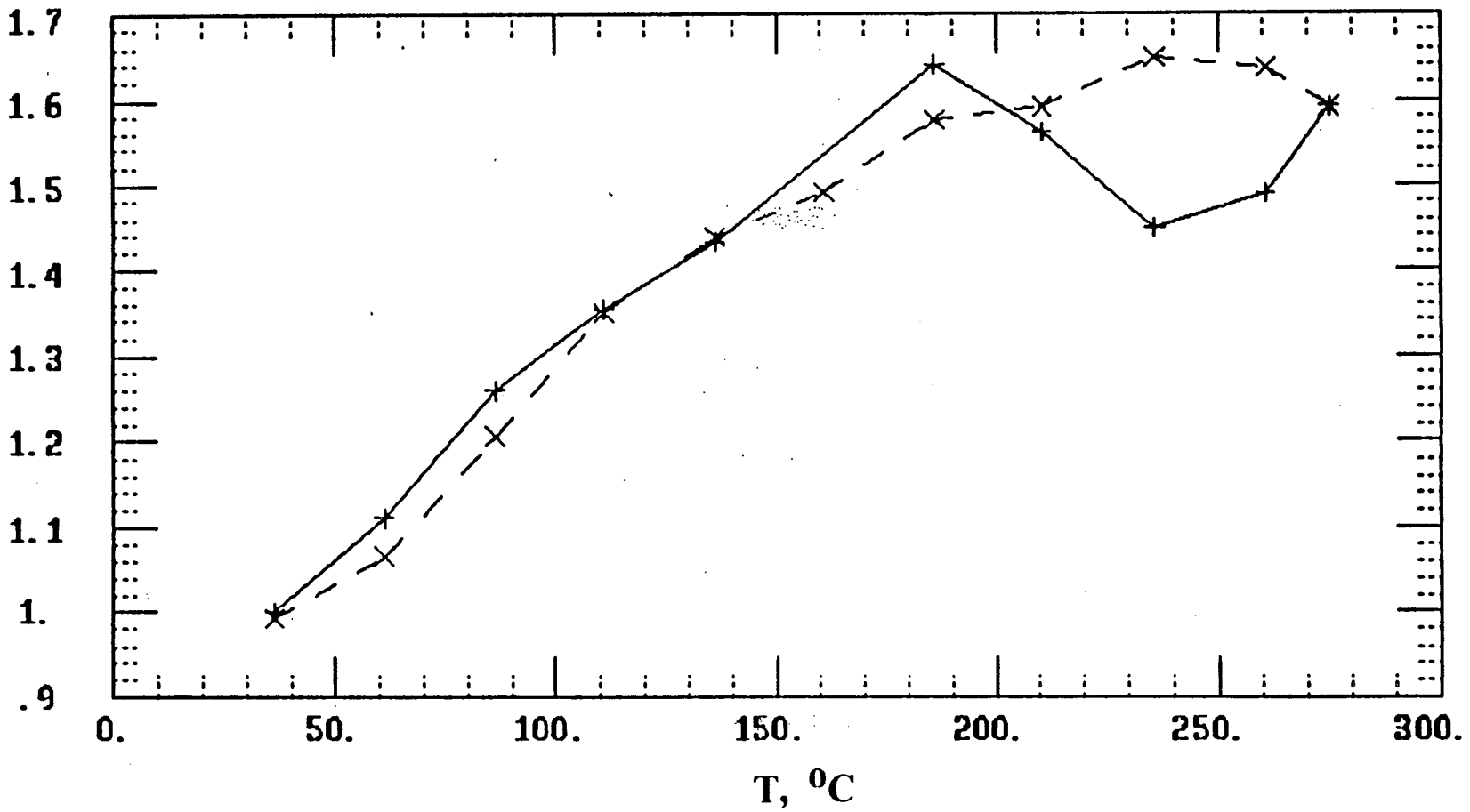

Figure 10. Relative values of Electron Density Variance for the SAXS heating experiment of Figure 6, polyurethane L. Solid line (+): ascending temperatures; dashed line (X): descending temperatures.

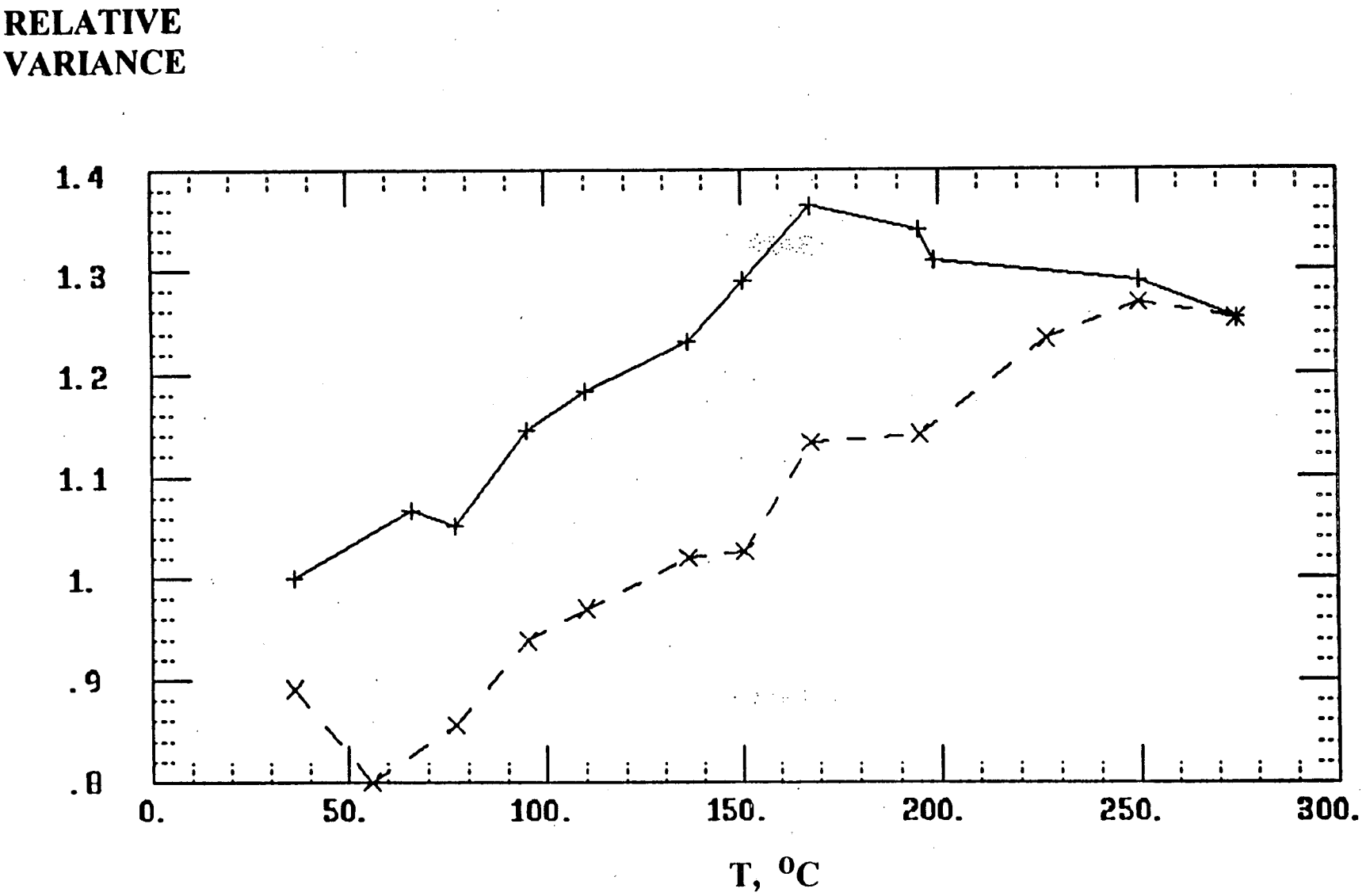

Figure 11. Packing diagram of the model compound $C_{10}H_{18}N_2O_4$, CHDI end-capped with methanol, based on Jasinski[24]; space group P21/C. Lattice parameters: a = 1.0563 nm, b = 0.7265 nm, c = 0.8375 nm; Beta = 106.87°.

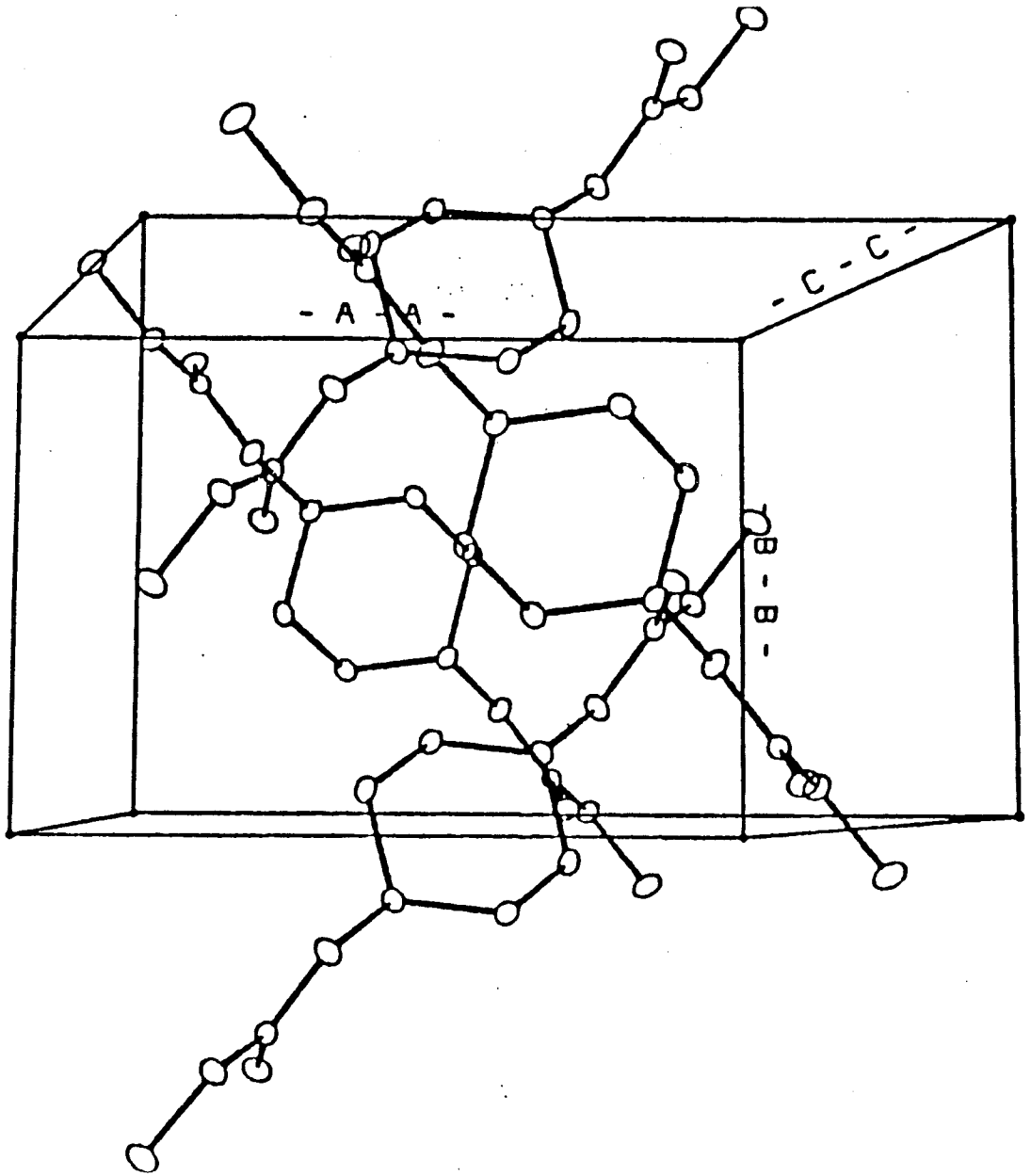

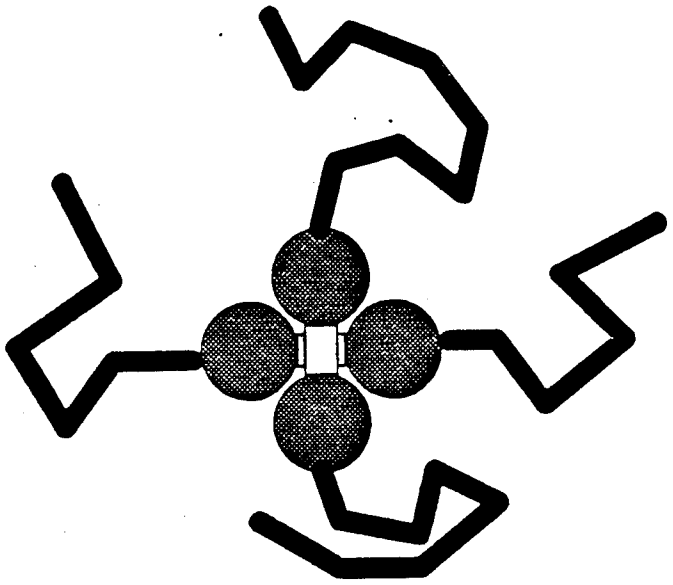

Figure 12. Proposed packing of -CHDI-BD-CHDI- hard segment dimers in analogy to the model compound structure of Figure 11. The spheres represent the cyclohexyl residues; the connecting bars, the urethane / aliphatic linkages. The solid broken lines surrounding the dumbbells represent the soft segments.

Figure 12.

Table 1. CHDI Polyurethane Compositions

Sample	Molar Composition			PTMO	NCO/OH	Wt. Fract. Hard Seg.
	CHDI	PTMO	BD	M_n	Molar Ratio	(M_H)
A	2.125	1.0	1.5	2033	0.85	0.188
B	2.250	1.0	1.5	2033	0.90	0.194
C	2.375	1.0	1.5	2033	0.95	0.200
D	2.500	1.0	1.5	2033	1.00	0.206
E	2.625	1.0	1.5	1934	1.05	0.221
F	2.750	1.0	1.5	1934	1.10	0.227
G	2.875	1.0	1.5	2033	1.15	0.224
H	3.000	1.0	1.5	2033	1.20	0.230
I	3.000	1.0	2.0	1934	1.00	0.252
J	4.000	1.0	3.0	1934	1.00	0.317
K	2.000	1.0	1.0	2862	1.00	0.122
L	4.000	1.0	3.0	2862	1.00	0.239
M	5.000	1.0	4.0	2862	1.00	0.286

Table 2. Definition of Terms for Small Angle X-ray Scattering

λ	X-ray wavelength, nm or Å at the discretion of the user.
2θ	Scattering angle, radians, for an individual intensity datum.
a	Sample-to-detector distance, cm.
A_s	Attenuation ratio for the sample, dimensionless.
C_k	Physical constant involving Avogadro's number and the Thomson scattering constant for an electron having the value $8.34 \cdot 10^{-3}$ $cm^3/mole^2$; from Kratky[26].
D	Sample thickness, cm.
I(q)	Intensity measured at the indicated value of the scattering variable q, using pinhole optics.
$I_K(m)$	Intensity taken as a function of Kratky's[26] preferred scattering variable m, using pinhole optics.
I(q)	Intensity measured at the indicated value of the scattering variable q, using slit optics.
$I_K(m)$	Intensity taken as a function of Kratky's[26] preferred scattering variable m, using slit optics.
m	Kratky's scattering variable: the distance in the registration plane from the primary beam to a particular detection position, cm.
P_0	Primary beam power incident on the sample.
P_s	Primary beam power as attenuated by the sample.
P_{std}	Power (incident on the sample) of a hypothetical standard primary beam of constant intensity.
q	Scattering variable $(4\pi/\lambda) \sin \theta$, units are inverse of the units of λ.
ρ_e	Electron density, moles e^-/cm^3; its fluctuation in space gives rise to X-ray scattering.

Table 3. Definitions for Electron Density Variance Calculations

Symbol	Units	Definition
$\langle\Delta\rho_e^2\rangle$	(moles e^-/cm^3)^2	Variance (mean squared variation from the average value) of the electron density: with no corrections applied, this represents the variance of a real system with diffuse domain boundaries and statistical density fluctuations within the microphases, as in Fig. 4c of Bonart and Muller.[4]
$\langle\Delta\rho_e^2\rangle'$	(moles e^-/cm^3)^2	Electron density variance value of a system corrected for fluctuations within the microphases, but not for diffuse microphase boundaries, as in Fig. 4b of Bonart and Muller.[4]
$\langle\Delta\rho_e^2\rangle''$	(moles e^-/cm^3)^2	Electron density variance value of a system corrected for both fluctuations within the microphases and for diffuse microphase boundaries, as in Fig. 4a of Bonart and Muller.[4]
$\langle\Delta\rho_e^2\rangle_P$	(moles e^-/cm^3)^2	Electron density variance value of a fully microphase separated system.#
M_H	g/cm^3	Mass fraction of hard segment species.
M_S	g/cm^3	Mass fraction of soft segment species.
R_H	moles e^-/g	For hard segment: conversion factor* from mass density to electron density.
R_S	moles e^-/g	For soft segment: conversion factor* from mass density to electron density.
ϕ_H	dimensionless	Volume fraction of hard segment microphase.
ϕ_{HP}	dimensionless	Volume fraction of hard segment microphase of a fully separated system.#
ϕ_S	dimensionless	Volume fraction of soft segment microphase.
ϕ_{SP}	dimensionless	Volume fraction of soft segment microphase of a fully separated system.#
μ_H	g/cm^3	Mass density of hard segment microphase.
μ_{HP}	g/cm^3	Mass density of hard segment microphase of a fully separated system.#
μ_S	g/cm^3	Mass density of soft segment microphase.
μ_{SP}	g/cm^3	Mass density of soft segment microphase of a fully separated system.#
ρ_H	moles e^-/cm^3	Electron density of hard segment microphase.
ρ_{HP}	moles e^-/cm^3	Electron density of hard segment microphase of a fully separated system.#
ρ_S	moles e^-/cm^3	Electron density of soft segment microphase.
ρ_{SP}	moles e^-/cm^3	Electron density of soft segment microphase of a fully separated system.#

* Such conversion factors are simply the ratios of the total atomic number to the total atomic weight for the species in question.

A fully microphase separated system is an idealized system consisting of pure hard and soft segment microphases with sharp microphase boundaries.

Table 4. Results of SAXS Interfacial Thickness Determinations from Slopes of Koberstein Plots: CHDI-Based Elastomer Samples

Sample	Koberstein[31] Slope * $nm^{-1.81}$	Interfacial Thickness σ * nm
A	0.0003	--N/A--
B	-0.0004	0.01
C	0.00008	--N/A--
D	-0.0006	0.01
E	-0.0007	0.02
F	0.0043	--N/A--
G	-0.0029	0.03
H	-0.0071	0.05
I	-0.0015	0.02
J	-0.045	0.15
K	-0.0009	0.02
L	-0.014	0.08
M	-0.045	0.15

N/A: a positive slope will not yield a thickness value.

* Thickness determinations from Koberstein[31] plot curve fit, using range of $q^{1.81}$ = 2.30 to 3.25 $nm^{-1.81}$, corresponding to q = 1.6 to 1.9 nm^{-1}.

Table 5. SAXS Results on Lupolen Calibration Sample

Data Set No.	Koberstein[31] Slope [a] $nm^{-1.81}$	Interfacial Thickness σ nm	$\langle(\Delta\rho_e)^2\rangle \times 10^3$ [b] (moles $e^-/cm^3)^2$
1	-0.55_2	0.61	1.48_3
2	-0.53_7	0.60	1.46_3
3	-0.49_1	0.57	1.48_6

a. Curve fit range: from $q^{1.81} = 0.80$ to 1.09 $nm^{-1.81}$, corresponding to $q = 0.88$ to 1.05 nm^{-1}.

b. Experimental electron density variance value.

Table 6. Results of Iterative Calculation to Obtain Hard Segment Phase Densities from Experimental Electron Density Variance Values

Sample	Data for Iteration	Iterative Calculation Results			Inhomogeneity Lengths			Electron Density Variance Calculation **	
		Estimated Hard Segment							
	Expt. Variance $\langle(\Delta\rho_e)^2\rangle \times 10^3$ [a] (moles $e^-/cm^3)^2$	Vol. Fr. ϕ_{HP} (vol/vol)	Mass Dens. μ_{HP} (g/cm^3)	Elec. Dens. ρ_{HP} (moles e^-/cm^3)	Total L_C nm	Hard L_H nm	Soft L_S nm	Calcd. Variance $\langle(\Delta\rho_e)^2\rangle_p \times 10^3$ [b] (moles $e^-/cm^3)^2$	Expt. / Calcd Variance Ratio
A	3.18	0.152	1.358	0.703	2.25	2.66	14.8	3.15	1.01
B	3.29	0.157	1.361	0.704	2.62	3.11	16.6	3.21	1.02
C	3.31	0.163	1.359	0.702	2.59	3.10	15.9	3.27	1.01
D	3.22	0.169	1.352	0.698	2.64	3.17	15.7	3.32	0.97
E	3.49	0.181	1.357	0.700	2.72	3.32	15.0	3.49	1.00
F	3.64	0.186	1.361	0.701	2.85	3.51	15.3	3.54	1.03
G	3.41	0.185	1.354	0.697	2.94	3.60	16.0	3.48	0.98
H	3.42	0.190	1.352	0.695	3.06	3.77	16.1	3.53	0.97
I [c]	3.53 [c]	0.210 [c]	1.338 [c]	0.692 [c]	2.58	3.25	12.4	3.98 [c]	0.89 [c]
J [c]	3.95 [c]	0.270 [c]	1.327 [c]	0.688 [c]	3.13	4.26	11.8	4.81 [c]	0.82 [c]
K	2.14	0.100	1.363	0.701	2.61	2.89	26.2	2.06	1.04
L [c]	3.52 [c]	0.198 [c]	1.341 [c]	0.695 [c]	3.43	4.26	17.5	3.89 [c]	0.90 [c]
M [c]	3.44 [c]	0.243 [c]	1.316 [c]	0.683 [c]	3.69	4.84	15.6	4.52 [c]	0.76 [c]

a. Experimental electron density variance.

b. Calculated electron density variance.

c. Polymers in which the ratio moles BD / moles PTMO is 2.0 or greater.

d. Using μ_H = 1.357 g/cm^3 from the iterative calculation, excluding samples marked with c.

DISTRIBUTION LIST

No. of Copies	To
1	Office of the Under Secretary of Defense for Research and Engineering, The Pentagon, Washington, DC 20301
	Director, U.S. Army Research Laboratory, 2800 Powder Mill Road, Adelphi, MD 20783-1197
1	ATTN: AMSRL-OP-SD-TP, Technical Publishing Branch
1	AMSRL-OP-SD-TA, Records Management
1	AMSRL-OP-SD-TL, Technical Library
	Commander, Defense Technical Information Center, Cameron Station, Building 5, 5010 Duke Street, Alexandria, VA 23304-6145
2	ATTN: DTIC-FDAC
1	MIA/CINDAS, Purdue University, 2595 Yeager Road, West Lafayette, IN 47905
	Commander, Army Research Office, P.O. Box 12211, Research Triangle Park, NC 27709-2211
1	ATTN: Information Processing Office
	Commander, U.S. Army Materiel Command, 5001 Eisenhower Avenue, Alexandria, VA 22333
1	ATTN: AMCSCI
1	AMCMI-IS-A
	Commander, U.S. Army Materiel Systems Analysis Activity, Aberdeen Proving Ground, MD 21005
1	ATTN: AMXSY-MP, H. Cohen
	Commander, U.S. Army Missile Command, Redstone Arsenal, AL 35809
1	ATTN: AMSMI-RD-CS-R/Doc
	Commander, U.S. Army - ARDEC, Information Research Center, Picatinny Arsenal, NJ 07806-5000
1	ATTN: AMSTA-AR-IMC, Bldg. 59
	Commander, U.S. Army Natick Research, Development and Engineering Center Natick, MA 01760-5010
1	ATTN: SATNC-MI, Technical Library
1	SATNC-AI
	Commander, U.S. Army Satellite Communications Agency, Fort Monmouth, NJ 07703
1	ATTN: Technical Document Center
	Commander, U.S. Army Tank-Automotive Command, Warren, MI 48397-5000
1	ATTN: AMSTA-ZSK
1	AMSTA-TSL, Technical Library
1	AMSTA-SF
	President, Airborne, Electronics and Special Warfare Board, Fort Bragg, NC 28307
1	ATTN: Library

No. of Copies	To
	Director, U.S. Army Research Laboratory, Weapons Technology, Aberdeen Proving Ground, MD 21005-5066
1	ATTN: AMSRL-WT
2	Technical Library
	Commander, Dugway Proving Ground, UT 84022
1	ATTN: Technical Library, Technical Information Division
	Commander, U.S. Army Research Laboratory, 2800 Powder Mill Road, Adelphi, MD 20783
1	ATTN: AMSRL-SS
	Director, Benet Weapons Laboratory, LCWSL, USA AMCCOM, Watervliet, NY 12189
1	ATTN: AMSMC-LCB-TL
1	AMSMC-LCB-R
1	AMSMC-LCB-RM
1	AMSMC-LCB-RP
	Commander, U.S. Army Foreign Science and Technology Center, 220 7th Street, N.E., Charlottesville, VA 22901-5396
3	ATTN: AIFRTC, Applied Technologies Branch, Gerald Schlesinger
	Commander, U.S. Army Aeromedical Research Unit, P.O. Box 577, Fort Rucker, AL 36360
1	ATTN: Technical Library
	U.S. Army Aviation Training Library, Fort Rucker, AL 36360
1	ATTN: Building 5906-5907
	Commander, U.S. Army Agency for Aviation Safety, Fort Rucker, AL 3636
1	ATTN: Technical Library
	Commander, Clarke Engineer School Library, 3202 Nebraska Ave., N., Fort Leonard Wood, MO 65473-5000
1	ATTN: Library
	Commander, U.S. Army Engineer Waterways Experiment Station, P.O. Box 631, Vicksburg, MS 39180
1	ATTN: Research Center Library
	Commandant, U.S. Army Quartermaster School, Fort Lee, VA 23801
1	ATTN: Quartermaster School Library
	Naval Research Laboratory, Washington, DC 20375
1	ATTN: Code 6384
	Chief of Naval Research, Arlington, VA 22217
1	ATTN: Code 471
	Commander, U.S. Air Force Wright Research and Development Center, Wright-Patterson Air Force Base, OH 45433-6523
1	ATTN: WRDC/MLLP, M. Forney, Jr.
1	WRDC/MLBC, Mr. Stanley Schulman

No. of Copies	To
	U.S. Department of Commerce, National Institute of Standards and Technology, Gaithersburg, MD 20899
1	ATTN: Stephen M. Hsu, Chief, Ceramics Division, Institute for Materials Science and Engineering
1	Committee on Marine Structures, Marine Board, National Research Council, 2101 Constitution Avenue, N.W., Washington, DC 20418
1	Materials Sciences Corporation, Suite 250, 500 Office Center Drive, Fort Washington, PA 19034
1	Charles Stark Draper Laboratory, 555 Technology Square, Cambridge, MA 02139
	General Dynamics, Convair Aerospace Division, P.O. Box 748, Fort Worth, TX 76101
1	ATTN: Mfg. Engineering Technical Library
	Plastics Technical Evaluation Center, PLASTEC, ARDEC, Bldg. 355N, Picatinny Arsenal, NJ 07806-5000
1	ATTN: Harry Pebly
1	Department of the Army, Aerostructures Directorate, MS-266, U.S. Army Aviation R&T Activity - AVSCOM, Langley Research Center, Hampton, VA 23665-5225
1	NASA - Langley Research Center, Hampton, VA 23665-5255
	U.S. Army Vehicle Propulsion Directorate, NASA Lewis Research Center, 2100 Brookpark Road, Cleveland, OH 44135-3191
1	ATTN: AMSRL-VP
	Director, Defense Intelligence Agency, Washington, DC 20340-6053
1	ATTN: ODT-5A, Mr. Frank Jaeger
	U.S. Army Communications and Electronics Command, Fort Monmouth, NJ 07703
1	ATTN: Technical Library
	U.S. Army Research Laboratory, Electronic Power Sources Directorate, Fort Monmouth, NJ 07703
1	ATTN: Technical Library
	Director, U.S. Army Research Laboratory, Watertown, MA 02172-0001
2	ATTN: AMSRL-OP-WT-IS, Technical Library
20	Authors